Tunable Absolute Capacitive MEMS Pressure Sensor on a Pure Play Commercial Process

Charles Allan
Bioelectrical Engineering, Electrical & Computer Engineering,
McGill University, Montreal
8-1-2015

A thesis submitted to McGill University in partial fulfillment of the requirements of the degree of Masters of Engineering

Abstract

A new method for manufacturing absolute MEMS (microelectromechanical systems) capacitive pressure sensors was developed using MIDIS^{TM}, a commercially available Pure Play process offered by Teledyne DALSA. The method takes advantage of the clean vacuum and low leak rate of 45 molecules/s ($7.5E^{-13}$ atm·cc/s) [2, 3] as a highly stable reference. The method allows absolute capacitive pressure sensors to be manufactured alongside 3-axis accelerometers and 3-axis gyroscopes opening the possibility of 10-axis IMUs on a single dye [4]. A method for characterizing the mechanical properties of the sensing membrane using FT-MTA02 Micromechanical Testing and Assembly Station by FemtoTools showed an accurate correlation of membrane deflection constant with simulated results. Finally, a testing set up was designed and built to measure the electrical performance of the pressure sensors under the biomedical, environmental and energy extraction applications. This pressure testing set up will be used to compare sensor data from sensors with diameters ranging from 210-360um with membrane thicknesses of 3 and 5um. The data will be valuable in showcasing the range and versatility of this method for manufacturing absolute pressure sensors. From the simulations we expect our sensors to have a resolution of 0.01kPa with an accuracy of +/-0.7% in the smallest package (2mmx2mmx0.8mm) while consuming only 24uA in high resolution and 3.3uA in low resolution. A high performance, low power, customizable pressure sensor that can be fabricated alongside accelerometers, gyroscopes allowing for 10-axis IMUs on a single dye.

Abrégé

Une nouvelle méthode pour fabrique des capteurs de pression MEMS absolue a été développée sur la plateforme MIDIS^{TM}. MIDIS^{TM} est un procédé commercial offert par Teledyne DALSA. Les capteurs de pression MEMS utilise le vide ultra base avec un taux de fuite ultra base de 45 molécules par seconde [2, 3] comme référence ultra stable. Cette méthode de fabrication est aussi compatible avec les accéléromètres 3 axes et les gyroscopes 3 axes, ouvrent la possibilité de fabriqué des systèmes de mesure inertiel (SMI) de 10 axes dans un puce [4]. Une méthode pour caractériser les propriétés mécanique de la membrane est introduite. La méthode utilise le FT-MTA02 de FemtoTools. La méthode montre une bonne corrélation de la constante de déflection entre les mesures et les simulations. Une méthode pour mesurer la performance électrique des capteurs de pression est aussi introduite. Cette méthode va être utilisée pour caractériser des capteurs avec des diamètres de 210-360um et épaisseurs de membranes de 3 et 5um. Cette information sera utiliser pour montre la versatilité de cette méthode de fabrication de capteurs de pression MEMS absolue. Les capteurs devront détecter résolution de 0.01kPa avec une précision de +/-0.7% dans un emballage de seulement 2mmx2mmx0.8mm. Le capteur consume seulement 24uA en haute résolution, et 3.3uA en bas résolution.

Acknowledgements

I would like to thank my advisor Professor Vamsy P. Chodavarapu. Ever since I joined the lab, he has been a great role model and guiding force behind my research. I'd also like to thank Dr. Edward Harvey for introducing me to this group and spiking my interest in the field of bioelectronics. I would also like to thank my engineering colleagues, George Xereas, Yucai Wang and especially Adel Merdassi for teaching me the art of microfabrication and helping me whenever I encountered difficulties.

I'd also like to thank Don Berry, Mathieu Nannini, John Li, Sasa Ristic and Lino Eugene for all their help and support in the Microfab at McGill. I'd also like to thank Sebastien Delprat for helping me at the INRS when systems were under repair at McGill.

Contents

Table of Figures

Introduction

Sensors are devices or systems that monitor various physical, chemical or biological parameters in the surrounding environment and provide representative signals that can be measured or stored [1, 5].The sensor signals can then be used by humans or robots to learn and act upon the surrounding environment. Thus, sensors essentially act like a bridge to transduce signals from one energy domain to another to help in easier detection, processing, storing and transmission [5].

Over the past several decades the rapid advancement in the semiconductor industry, has aggressively supported the miniaturization of physical sensors and led to the establishment of the field of Micro Electro-Mechanical Systems (MEMS) [6]. Today, MEMS based sensors including accelerometers, gyroscopes, pressure sensors, flow sensors and magnetic field sensors are found in applications spanning industrial process control, consumer electronics, environmental monitoring, avionics and aerospace, oil and gas exploration, and automobiles.

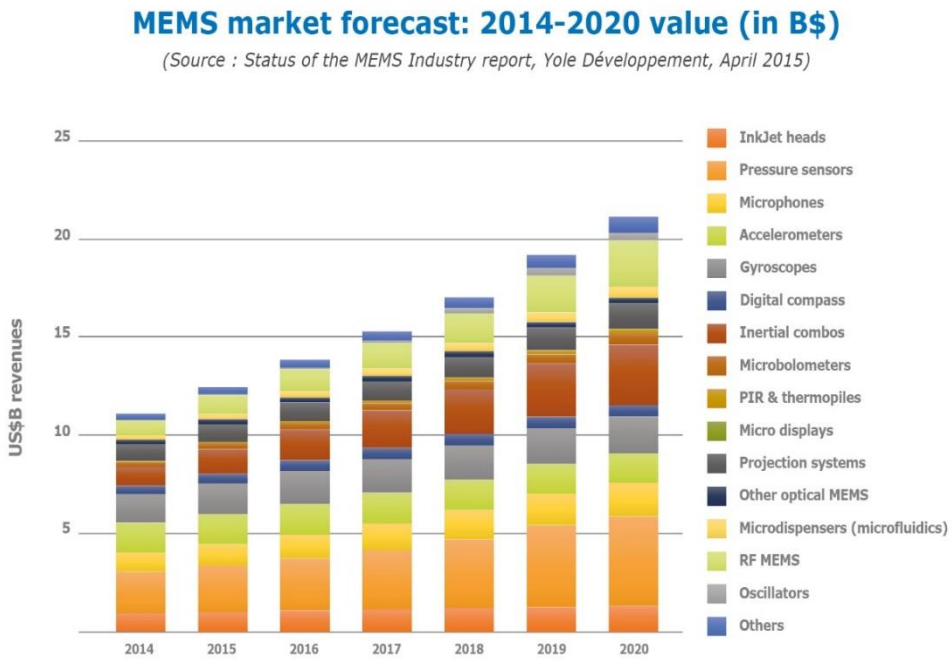

Figure 1 - MEMS market forecast (in $B) (April 2015) [4]

Yole Development predicts a growth of 13% compounded annually over the next five years [4]. In 2013, MEMS sensors represented an $11.1 Billion industry of which the largest component is pressure sensors at over $2 Billion [7].

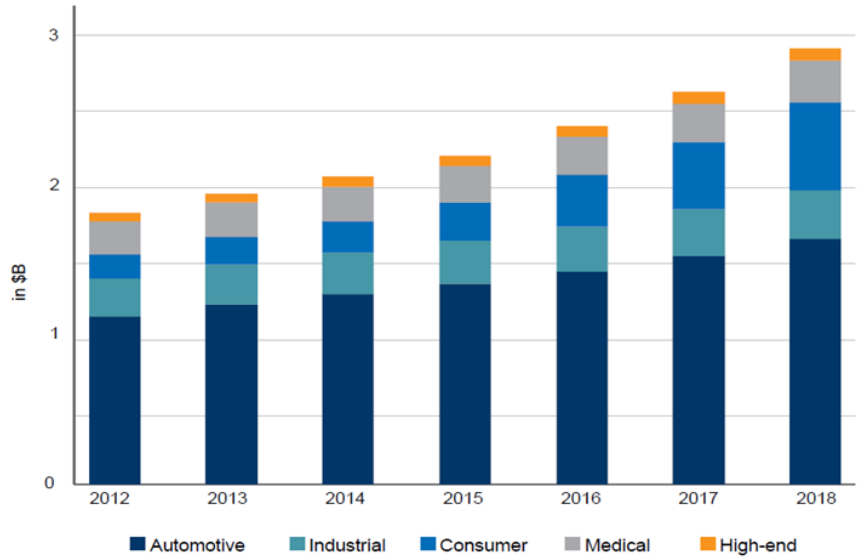

Figure 2 - MEMS Pressure Sensor Market Forecast, Yole Development [7]

In many industrial applications there is a need for miniaturized, high performance, low cost and low power consuming pressure sensors. Currently, the largest market for wireless MEMS pressure sensors is in the automobile industry for tire pressure monitoring [6] [4]. However, with the increased demand for wireless wearable devices, the consumer electronics industry is set to increase rapidly. The goal within this industry is to develop fully integrated 3-axis accelerometer, 3-axis gyroscope, 3-axis magnetometer and a pressure sensor within the same MEMS component. This is known as a 10-axis inertial measurement unit (IMU) [4]. Developing a 10-axis IMU has many challenges on the signal processing and MEMS sides. On the MEMS side, one of the challenges is developing a process that can integrate a pressure sensor alongside other MEMS components on a single chip [8]. Our goal with this research project was to develop a miniaturized, high performance, low cost and low power consuming pressure sensor that could be compatible within a single chip IMU system.

Due to the scope of the long term project, the development of the MEMS component was restricted to the pressure sensor. Below, we will describe the most commonly used transduction principles

that are also employed in many commercially available MEMS pressure sensors including piezoresistance, piezoelectric, resonant and electrostatic (or capacitive) [5].

Transduction Principles

Piezoresistance

Piezoresistance in one of the most widely exploited transducing principle for MEMS sensors [5]. The principle of piezoresistance was first discovered in 1856 by Lord Kelvin, who noted that when metals were placed under tensile stress there was a measurable change in resistance that was based on the type of the material used and was given by Equation (1),

$$R = \frac{pl}{A} \qquad (1)$$

where, R is resistance, p is the bulk resistivity constant, l is the length and A is the cross sectional area of the resistive device. The change in resistance can be derived from Equation (2), given that the cross sectional area *A* can be decomposed into its width and thickness.

$$\frac{dR}{R} = \frac{dp}{p} + \frac{dl}{l} - \frac{dt}{t} - \frac{dw}{w} \qquad (2)$$

For elastic materials, there is a correlation for strain based on the direction the stress is being applied (longitudinal vs. transverse). This correlation is known as Poisson's Ratio, *v*, and is typically around 0.3 (for Silicon it is 0.22) [9]. If we assume that, for small strains, the derivative is equivalent to change then,

$$\frac{dl}{l} = \frac{\Delta l}{l} = \varepsilon_l \quad (3)$$

$$\frac{dt}{t} = \frac{\Delta t}{t} = \varepsilon_t = \varepsilon_w = -v\varepsilon_l \quad (4)$$

$$\frac{\Delta R}{R} = \frac{\Delta p}{p} + \varepsilon_l + v\varepsilon_l + v\varepsilon_l = \frac{\Delta p}{p} + \varepsilon_l(1 + 2v) \quad (5)$$

In order to properly characterize sensing mechanisms a typical method is to quantify the transduction from the mechanical to electrical domain. This concept is known as the Gauge Factor.

$$G.F. = \frac{relative\ change\ in\ resistance}{applied\ strain} = \frac{\Delta R/R}{\varepsilon_l} = \frac{\Delta p/p}{\varepsilon_l} + (1 + 2v) \quad (6)$$

The early sensors that used piezoresistance were made of thin metal and are known as strain gauges[10]. The Gauge Factor of strain gauges are dominated by the second term in the Equation (6), which was caused by small changes in geometry [5].

The Gauge Factor of semiconductor based devices are dominated by the change in bulk resistivity known as the piezoresistive effect. When P-type Si is compressed, the number of holes decreases causing an increase in resistance [8]. While N-type silicon demonstrates an opposite effect due to the increased electron mobility, lowering the resistance. Piezoresistive devices by definition have much larger gauge factors than metal strain gauge devices [5].

These large gauge factors enable a drastic reduction in size of the sensors while increasing performance. This size reduction as well as the advent of batch manufacturing capabilities borrowed from the semiconductor industry reduces the cost of these devices [5]. These advantages have propelled piezoresistive devices to the wide market share they now hold [4].

Table 1- Gauge Factor of several Piezoresistive Materials[5]

Material type	Gauge Factor
Metal Foil	2-5
Thin Metal	2
Single Crystal Silicon	-125 to 200
Poly-Silicon	±30
Thick Film	10

One of the drawbacks of piezoresistive strain gauges is that they are very susceptible to changes in temperature [5].

$$\frac{\Delta R}{R} = GF\varepsilon_l + \alpha T \qquad (7)$$

To reduce the effect of temperature, αT, and amplify the resulting signal, the elements of the transducer are typically arranged in a half or full Wheatstone bridge configuration.

Piezoelectric

Piezoelectric materials are characterized by a change in electric charge when stressed [5]. The transducing effect is caused by a charge asymmetry within the crystal structure of piezoelectric materials, known as non-centrosymmetric materials such as lead zirconate titanate. In addition, a set of polymers were engineered to display this effect that include Polyvinylidene Fluoride (PVDF) [11] . PVDF is known as a ferroelectric since an external electric field must be applied first to pole the material for the effect to take place.

Piezoelectric materials are characterized by their ability to convert a given applied stress into an electric charge, known as their charge coefficient d_{ij} (C/N) [11]. As denoted by the subscripts ij the materials charge coefficient is highly dependent on the direction of the applied force.

$$Q = d_{ij}\, F_{ij} \quad (8)$$

From this charge equation, a voltage can be calculated by knowing the relative permittivity of the piezoelectric and dimensions of the element. Most notably the thickness between both contact electrodes and their surface area, A.

$$V = \frac{Q}{C} = \frac{d_{ij}F_{ij}t}{\varepsilon_o\varepsilon_r A} \qquad (9)$$

As sensors, piezoelectric devices are interesting since a voltage can be measured directly from the output without a complex signal processing interface that is needed with most transducing mechanisms. These materials have been popularized more recently as a way to harvest energy from vibration [11]. However, it has been well documented that changes in temperature will affect the materials charge coefficient. This effect can be quite substantial, attribute to increased mobility

to the atoms within the crystallographic structure. This is known as the pyroelectric effect, and it has been exploited to create infrared sensors [5, 11].

Table 2 – Charge Coefficient and Relative Permittivity of Several Piezoelectric Materials [8]

Material	Form	d_{zz}(pC/N)	Relative Permittivity (ε_r)
Quartz	Single Crystal	2	4
PVDF	Polymer	20	12
Barium Titanate	Ceramic	190	2,000
PZT	Ceramic	300-600	400-3,000
Zinc Oxide	Single Crystal	12	12
Lithium Niobate	Single Crystal	6-16	30

Resonance

Resonators work on the principle that the frequency of vibration of a resonating mechanical structure varies as a function of the external applied stimulus [12]. The magnitude of the displacement of the resonating structure is ultimately dependent on the damping effects acting on the system. Resonators are designed to have large vibrations at very specific natural frequencies. The narrower the bandwidth, the better the performance of the resonator becomes for a given frequency range. In order to quantify this performance, a term known as the quality factor (Q-factor) is used. In practice this term is defined as Equation (10),

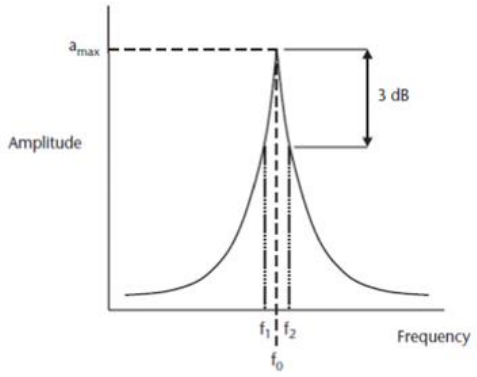

Figure 3- Frequency Response Curve [5]

$$Quality\ Factor = \frac{f_0}{\Delta f} \quad (10)$$

The quality factor is limited by various mechanisms that absorb energy. The Quality factor is dependent on three main causes: energy lost to surrounding fluid (Q_f), energy that is absorbed by the resonator's supports (Q_s), energy dissipated internally within the resonator's material (Q_m). Minimizing these effects have been the focus of research for many years in order to maximize the performance of the resonator.

$$\frac{1}{Q} = \frac{1}{Q_f} + \frac{1}{Q_s} + \frac{1}{Q_m} \quad (11)$$

From the factors that affect the performance of the resonator, the energy lost to the fluid and the energy loss of the support structure can be minimized, while the energy lost to the material is a limitation of any bulk material [13]. Placing the resonator within a vacuum can mitigate the energy lost to the fluid. The energy lost by the supports can be reduced through strategic design [14]. By proper understanding of modes, the support structures could be placed in places where motion is minimal in vibrational dynamics that are known as inflection points. The most common resonating mechanisms will be outlined below [5, 14, 15].

Bulk Wave Oscillators

Bulk Acoustic Wave (BAW) oscillators function in different modes that are dependent on the orientation the electrodes in relation to the crystal structure[14]. Quartz crystal is widely used for the development of bulk mode oscillators. In practice, this is controlled by the orientation the

crystal is cut. AT-cut crystals produce Thickness Shear Mode (TSM) resonating devices also known as quartz micro-balance, this is the most common type of bulk wave oscillator. These devices are widely used as frequency references for electronic oscillators. Over the past few decades, they have also been used for chemical and biological sensing.

The natural frequency of BAW-TSM is a function of the shear wave phase velocity and the thickness of the piezoelectric as given by Equations (13) below,

$$f_N = \frac{N v_s}{2t} \qquad (12)$$

$$v_s = \left(\frac{\mu_q}{\rho_q}\right)^{1/2} \qquad (13)$$

where, μ_q is the shear stiffness and ρ_q is the mass density. Therefore, the shear velocity is a function of the properties of the cut crystal [16]. For AT-cut quartz, the shear velocity is $3.34 \times 10^5 cm/s$. From Equation (12), in order to increase the fundamental frequency of the transducer, the thickness must be reduced. Limitations in handling of thin quartz wafers result in a frequency range between 10-50 MHz [13, 14, 16].

Surface Acoustic Wave (SAW) Oscillators

SAW sensors rely on the modulation of acoustic waves on the surface to sense physical phenomenon. The sensor transduces an electrical signal into a mechanical wave which can be easily influenced by external physical or chemical phenomenon, this wave is captured by a sensing transducer that converts the wave back to the electrical domain. Changes in amplitude, phase, frequency, or time-delay are used to quantify the physical phenomenon in question.

Since the voltage differential signal is only applied to one surface in form of interdigitated electrodes, the mechanical signal is concentrated on that surface. The number of comb teeth used in the electrode and the voltage of the signal both increase the strength of the signal and overall performance. Acoustic absorbers are placed on the extremes of the device in order to limit the amount of noise picked up by signal reflections (i.e. echoes). This technique was first

demonstrated by White in 1965 to better understand traveling wave properties through an elastic material [13, 16]. SAW technology gained mass recognition in telecommunication for high frequency signal filtering.

The energy of the propagating wave is concentrated at the surface of the SAW sensor. This means the wave is highly sensitive to any physical changes at the surface. Wohltjen et al. [17] were the first to demonstrate the potential of SAW as a sensing mechanism, by applying gas sensitive polymer films to the surface of the devices. The polymer would change properties by swelling when exposed to certain gases, applying more load on the surface of SAW device and thereby attenuating the traveling wave.

Capacitance

Capacitive or electrostatic sensing is one of most widely used principles for the development of MEMS sensors in modern consumer electronics and mobile devices [18]. Capacitive sensing devices are relatively easy to manufacture, provide an accurate method of sensing, relatively insensitive to temperature variations and provide low noise operation [7]. Capacitive sensors are made of one or more stationary electrodes and one or more moving electrodes. For a typical parallel plate capacitive structure, ignoring fringing effects, the capacitance is given by Equation (14),

$$C = \frac{\varepsilon_0 \varepsilon_r A}{d} \ (F) \quad (14)$$

where, ε_0 is the permittivity of free space, ε_r is the permittivity of the material between the plates, A is the overlapping surface area of both plates and d is the distance between the plates.

Capacitive MEMS pressure sensors typically consist of two parallel plate electrodes [19]. One electrode is able to deflect, while the other is fixed. For absolute sensing applications, there is a known pressure between the parallel plates. The difference in pressure on both sides of the flexible plate electrode, causes a gradient which leads to a deflection in the flexible electrode. There are many methods of making these devices [20-23]. One of the simplest methods, figure 4, involves fusion bonding two plates together with a cavity placed between them [24].

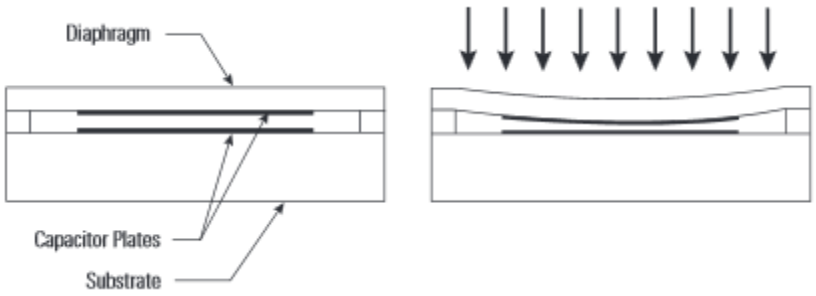

Figure 4- Parallel Plate Capacitive Pressure Sensor [24]

These type of devices are robust and less complex to fabricate. The challenge comes with getting electrical connections with the bottom fixed plate, without compromising the reference pressure between the parallel plates. These devices are excellent at detecting pressure changes over a small deflection range [18]. However, since the measurement principle is based on an inverse relationship with the gap distance ($\Delta C \approx \frac{1}{\Delta w(r)}$) as the deflection increases so does the membrane profile. The capacitance can be calculated from Equation (15) as,

$$C = \iint \frac{\varepsilon}{d - w(r)} \, r dr d\theta \qquad (15)$$

where $w(r)$ is the deflection at a given position. This result in a capacitance profiles similar to the Figure 5 shown below.

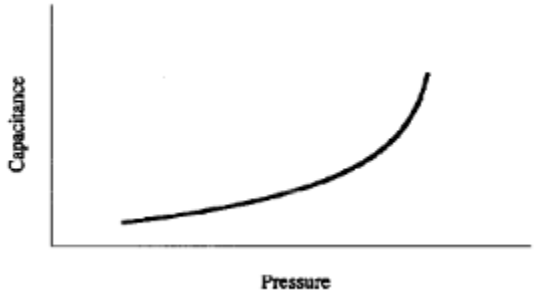

Figure 5 – Normal Mode Parallel Plate Capacitance Response [5]

To ensure the capacitance measurement remains within the linear range, the membrane must be designed with a thick membrane ($\frac{t}{w_{max}} < 5$). The nonlinearities can also be compensated electronically using a non-linear convertor circuit.

Limiting ourselves to MEMS design solutions, there are many other methods to increase the linear range of the pressure sensing device [19]. One method is to operate the pressure sensor within the touch mode range (TMCPS), this means that the membrane is in contact with electrically isolated fixed electrode [19].

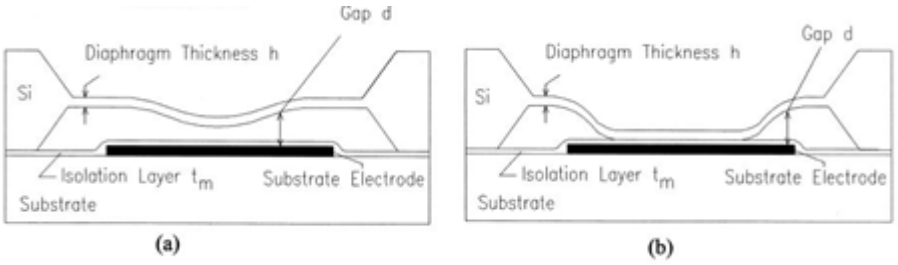

Figure 6 - Normal Mode (a) and Touch Mode (b) Working Profile [19]

Once the diaphragm comes into contact with the fixed electrode the transduction mechanism changes from gap distance based ($\Delta C \approx \frac{1}{\Delta w(r)}$) to contact surface area based ($\Delta C \approx \Delta A_c$) [5]. The slope of this relationship is related to the dielectric constant of the fixed electrode's insulating layer [19]. This relationship is linear over the TMCPS range as shown in Figure 7 below,

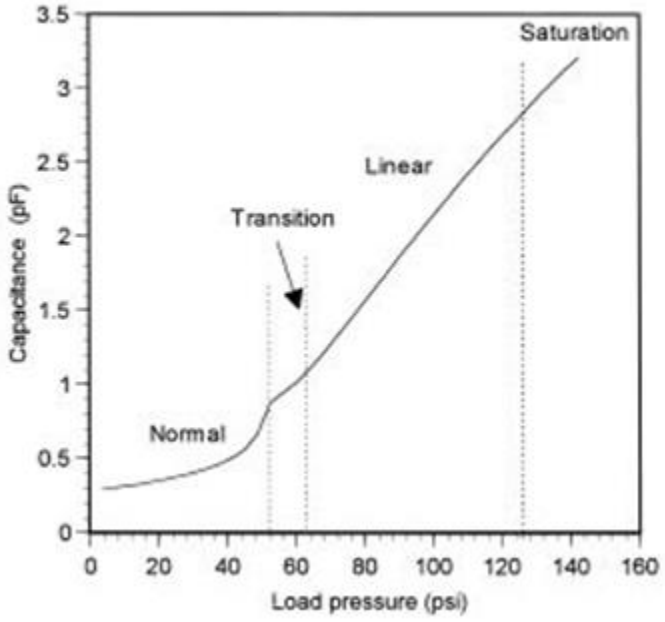

Figure 7 – Full Range Parallel Plate Response Curve [19]

The drawback of this technique is that it requires a minimum pressure before reaching its operating range [2, [19]. The preload pressure means that TMCPS is typically reserved for high pressure applications [19], which suits well as TMCPS has good overload protection. Another method to increase linearity is by using bossed or corrugated diaphragms as shown in Figure 8 below [25].

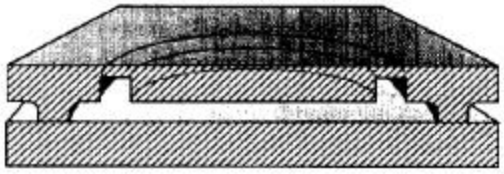

Figure 8 - Profile of Bossed Diaphragm [5]

A bossed diaphragms means the thicker center is much stiffer than the outer cutout [5]. The center will remain parallel to the fixed electrode as load is applied to the system [25]. Since the center section also contributes the most capacitance, the transducer behaves more like a parallel plate capacitor. Therefore the capacitance-pressure relationship will remain linear for a larger range than typical diaphragm based transducers [25, 26]. The issue with bossed diaphragms is that they begin to resemble mass-spring systems [25]. These mass-spring system can be subject to centrifugal force and mechanical shock/ vibration artifacts [5]. This is particularly important for pressure sensing in high noise environments [27].

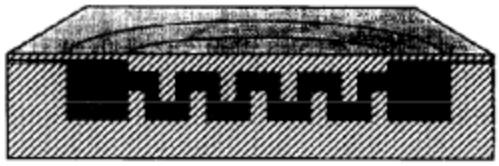

Figure 9 - Profile of Embedded Comb Diaphragm [5]

Figure 9 uses a comb design to increase linearity. The comb drive patterned on both the moving and fixed electrodes increase the surface area of the device. The principle uses change in overlapping surface area (A) to determine the capacitance of the system [5]. Each comb amplifies the signal resulting in a high signal to noise ratio [5]. Alignment and a stiff center are integral to functionality of this design. Any rotation or deflection will result in non-linear artifacts. This method increases the output signal density at a cost of manufacturing complexity.

Regardless of the implementation, capacitive pressure sensors require an interfacing circuit to convert the capacitive signal to an equivalent output voltage, frequency or digital readout [18, 19, 25]. The capacitance change is typically only a few femto Farads for a full scale signal [28]. In contrast, these device typically have parasitic loads on the order of several pico-Farads. Interfacing circuits must be capable of filtering out the capacitance signal from the noise. Excessive parasitic capacitance is a serious disadvantage, which slowed development of miniaturized capacitive sensors [29, 30]. Today, high performance capacitance to digital convertors are commercially available allowing for a resurgence of academic and commercial interest in the transduction mechanism [24].

Commercial MEMS Pressure Sensors

MEMS pressure sensors represent the largest market of all MEMS devices [7]. This gives us an excellent opportunity to study the structure and performance of many of the devices commercially available in the market.

General Electric NovaSensor

These pressure sensors are made entirely of silicon and rely on implanted piezoresistive sensors on the top of the sensing membrane to transduce the pressure signal. The first NovaSensor process was made from single <100> silicon wafer and had square membranes made by anistropically etching the backside of the device [1, 9]. The membrane thickness could be controlled using exposure time or doping the membrane to act like an etch stop [1]. Depicted below in Figure 10 is a sample of their first and second generation products.

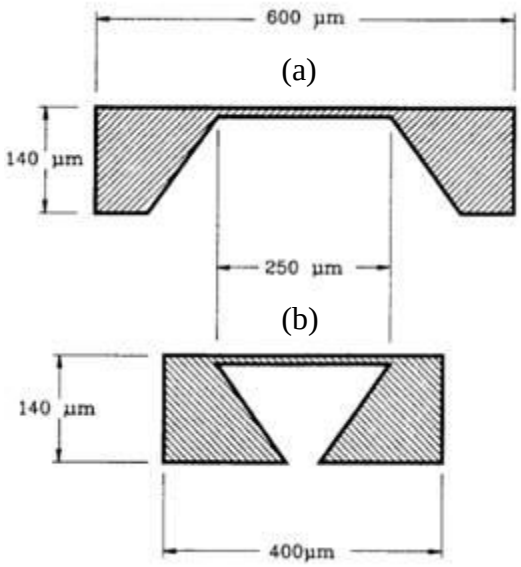

Figure 10 – NovaSensor's 1st generation (a) and 2nd generation (b) of Pressure Sensor Profile [1]

For space sensitive applications, NovaSensor released an improved device a few years later depicted in the Figure 10 above. These devices are made using a three stage process [1], first, the bottom cavity is etched out of bulk <100> silicon using an anisotropic etchant similar to KOH which is characterized by its 54.7^{o} sidewalls. A silicon on insulator wafer (SOI) is then fusion bonded to the bottom cavity silicon wafer. SOI wafers are essentially thin single crystal silicon membrane on thick handling wafers with an insulating layer of silicon dioxide that is used as an etch stop mechanism when releasing the membrane. The thickness of the membrane is determined by the SOI wafer chosen for the fusion bonding [1]. The handle wafer is etched back using isotropic etching, typically dry reactive ion etching is used to limit the problems with backside etching. Once the membrane is released, the final step requires ion implanting the piezoresistive elements [1]. The reduced footprint limits the number of piezoresistive elements that can be placed on the wafer to a half bridge configuration. This device has a reduced footprint when compared with the previous iteration because the anisotropic etching can be much narrower as the initial geometry is what will determine the sensing elements dimensions rather than the ending geometry from the original design. Another important element of this design is it can be made as a gauge or absolute pressure sensor depending on whether the bottom cavity is polished back or not [1, 8].

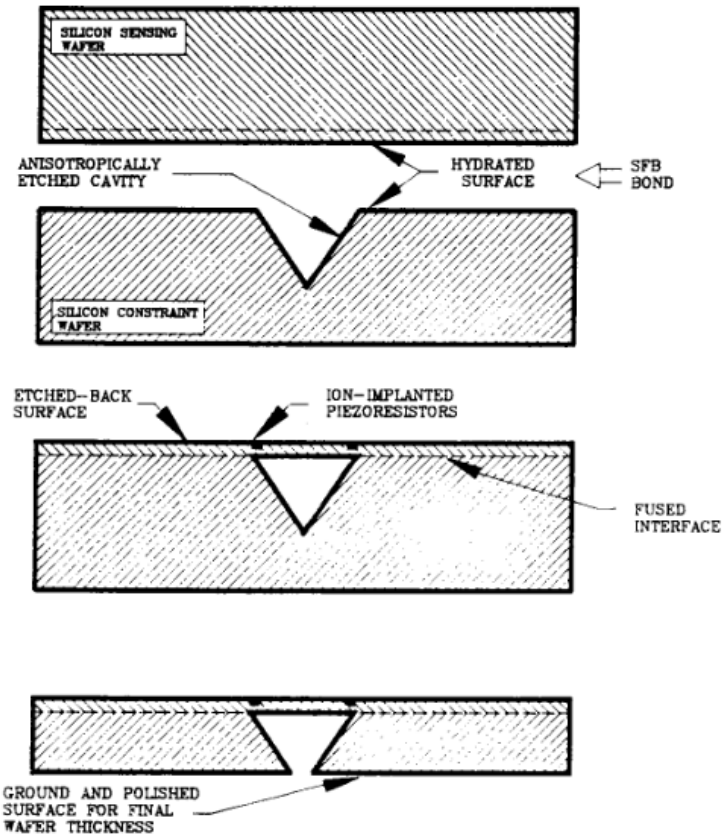

Figure 11- NovaSensor's 2nd Generation Fabrication Process [1]

Murata Electronics Oy

A mass produced silicon based bulk micromachined capacitive pressure sensor was developed by VTI Technologies [22]. This company was acquired by Murata in 2012. This device utilizes deflection mode capacitance sensing to measure pressure. The device targets low power and battery less applications such as tire pressure monitoring systems (TPMS) [22].

Like the second NovaSensor product, the device by Murata Electronics Oy is made of two separate wafers which are machined independently then fusion bonded together. The sensing membrane is etched using anisotropic wet etching [22]. This process was chosen because of its multi-wafer capabilities and precise etch quality. The most important aspect of Murata's design is how the etching mask is positioned [22, 23]. The etch mask is positioned to form a diamond shape in relation to the <110> crystallographic direction of the <100> silicon wafer. This method results in

(111) planes being located at the corner of the device membranes [22]. Placing the masks in the 110 orientation reduces the overall footprint of the membranes.

Figure 12 - Exploded View of Murata's Capacitive Pressure Sensor [22]

The smaller footprint allows for more sensors to be processed on a single wafer [23]. The silicon is then anisotropic wet etched using an anisotropic alkali etchant (KOH, EDP, NaOH or TMAH). The membrane dimensions are designed in such a way that sensor elements from 1bar (20um) to 30bar (80um) would be realized. By using wet etching the height of the diaphragm can be processed accurately [22]. Contrary to many fusion bonded designs, the 1um gap is machined into the bonding side of the membrane wafer. This 1um gap is held constant to keep a consistent capacitive dynamic range for all variants in diaphragm thickness [22]. This gap can be machined either using DRIE or anisotropic wet etching. DRIE enables round support structures which are favorable for accurate mechanical modeling of the devices. These membranes are then fusion bonded to a silicon support layer.

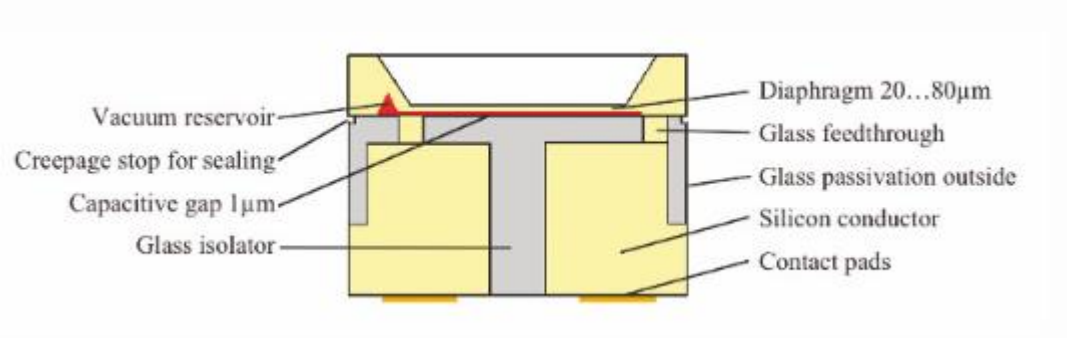

Figure 13- Profile of Murata's Capacitive Pressure Sensor [22]

In order for these devices to operate properly the membrane layer (sensing electrode) must be electrically isolated from the support wafer (fixed electrode), parasitic capacitance reduced and the reference pressure must be held constant. Murata isolates the top and bottom electrodes using Through Silicon Vias (TSVs). These TSVs are fabricated using a Bosch process which etches long narrow channels within the silicon support wafer. These channels are then filled with silicon dioxide either through a thermally grown or vapor deposition approach [22, 23]. The parasitic capacitance is reduced by widening the gap between the sensing elements such as the fixed and moving electrodes, and the connecting/support structure. Reducing the parasitic capacitance in turn reduces the device's temperature dependence making it almost negligible. The next challenge is ensuring a highly stable reference pressure. Glass has characteristics such as outgassing and adsorption of residual gasses on the glass surface. These effects are compensated by adding wet etched gas pockets connected to a larger reference pressure volume (vacuum reservoir) [22].

The electrical connections are placed on the backside of the device allowing them to be isolated from the sensing medium. After bonding the wafers together, the devices are separated as shown in Figure 13.

Freescale Semiconductor

Freescale Semiconductor process their pressure sensors directly alongside their CMOS circuitry in order to save space and limit the number of manufacturing steps [31]. Typically, the pressure sensor's fixed electrode is formed by a doped portion of silicon substrate. This area is doped at the same time as the source and drains of the CMOS transistors are being formed. The moving diaphragm is made of a vapor deposited polysilicon that is subsequently implanted and annealed

to dope the diaphragm and relieve the stress that formed during the deposition process [31, 32]. This annealing process affects the CMOS transistor characteristics and is one of the drawbacks of CMOS integrated pressure sensors. Freescale Semiconductor managed to get around this problem by simultaneously manufacturing the pressure sensor alongside the CMOS circuitry and changing the timing of certain critical steps [31, 32].

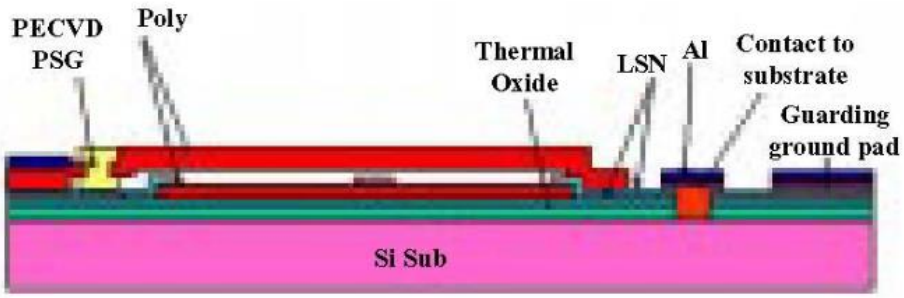

Figure 14- Freescale Surface Micro-machined Pressure Sensor [32]

The first characteristic of Freescale Semiconductor's approach is to make both the fixed electrode and the sensing electrode out of surface micro-machined doped polysilicon [32]. The fixed electrode is placed on a thin oxide simultaneously with the floating gate electrodes of an EEPROM cell. A sacrificial layer, typically low stress silicon rich nitride, is deposited on the fixed electrode. This sacrificial layer is between 0.2 and 1 micron thick. Following this step, the sensing diaphragm made of doped polysilicon is deposited. A channel is etched within in the diaphragm to access the sacrificial layer. The sacrificial nitride is then etched using buffered oxide etchant (BOE), releasing the diaphragm. These steps are done before implanting the source and drain areas of the CMOS transistors [32]. Delaying this annealing step allows for both the activation of the implant areas and the activation of the diaphragm to happen simultaneously [31]. Limiting the adverse doping effects. The activation annealing step is a rapid thermal process performed at a temperature between 900^{o} and 1100^{o} C.

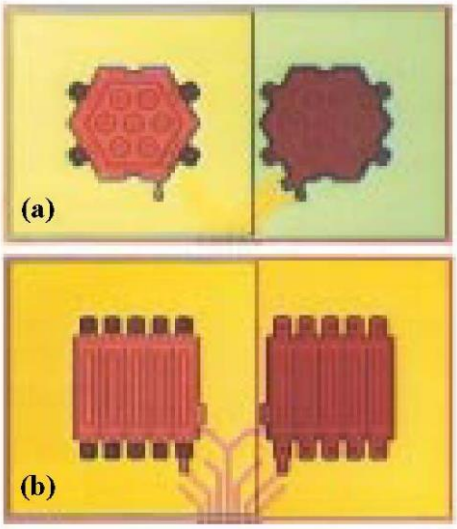

Figure 15- Top View of Freescale's Pressure Sensor [32]

This implementation is interesting because it can be made simultaneously with CMOS circuitry as described below. The problem is that the CMOS step sequence must be modified in order for this process to flow properly. Surface micro-machined pressure sensing devices allow for small controllable cavity thicknesses. This allows for the electrodes to be placed very close together, enhancing capacitance signal sensitivity. However, there are two factors that make these pressure sensors mechanically inferior to bulk micro machined sensors. The first aspect is that since this is an additive process, the best mechanical material that can be used to be compatible with CMOS processing is polysilicon [5, 9, 33]. Even when annealed, polysilicon inherently is an inferior material to single crystal silicon due to problems with hysteresis, lower yield stress and temperature dependence [27]. Another problem that plagues all surface micro-machined pressure sensing devices is the channel required for releasing the diaphragm [5]. This channel hole will always be present, and causes variability in performance and must be well designed to optimize batch yield. Batch yield is a very important factor in determining commercial success of MEMS product. One example is Tronics capacitive pressure sensor which had a surface micro-machined pressure sensor that had problems with batch yield due to sacrificial layer etching problems [27].

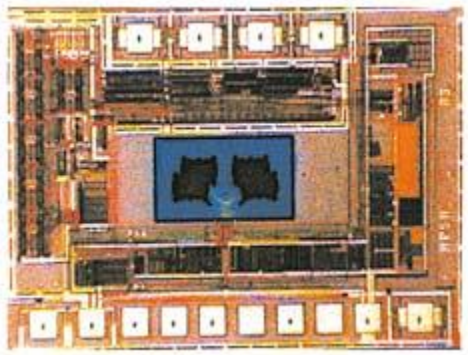

Figure 16- Freescale's Pressure Sensor with integrated CMOS circuitry [32]

Tronics Microsystems

One of the first capacitive pressure sensing devices based on surface micromachining was developed in 1993 led by Benard Diem at the *Commissariat a l'Energie Automique et aux Energies Alternatives* (CEA) [27]. This patented technology was later commercialized in 2002 by Tronics Microsystems. The absolute capacitive pressure sensor was developed for implantable biomedical sensing applications [34, 35]. Though its small dimensions (die size > 1.5mm^2) first made them very attractive, batch reliability plagued the commercial success of the product. The process begins with a separation by implantation of oxygen (SIMOX) wafer [34]. SIMOX uses an oxygen ion beam implantation process followed by high temperature annealing to create a buried silicon oxide layer [21].

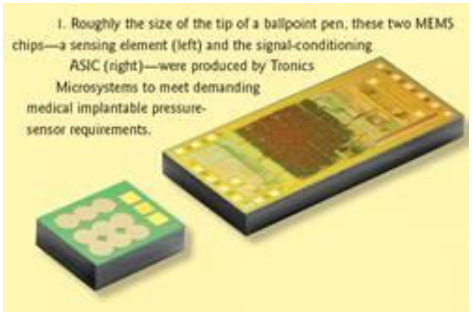

Figure 17- Tronics Pressure Sensor with CMOS circuitry [21]

The SIMOX wafer offers a commercially available cost effective method to have single crystal sensing layer with a buried oxide layer used as a sacrificial and insulating layer [34]. The process sequence illustrated below begins with 0.2um single crystal surface layer which is then thickened by depositing epitaxy silicon to 4um. An access hole is etched using dry or anisotropic wet etching in the membrane layer to access the buried silicon oxide. A selective section of Silicon Oxide is

wet etched in a hydrofluoric (HF) based solution beneath the openings made in the membrane layer [34]. This solution etches in an isotropic manner revealing concentrically propagated circular cavities releasing the membrane above. The gap is dependent on the thickness of the oxide layer (0.4um), which is highly reproducible in the SIMOX process. This small gap results in a high capacitance between the membrane and the fixed electrode below (20pf/mm^2). The etching holes are hermetically sealed under vacuum by plasma CVD deposition of non-stressed dielectric layer plugs [34].

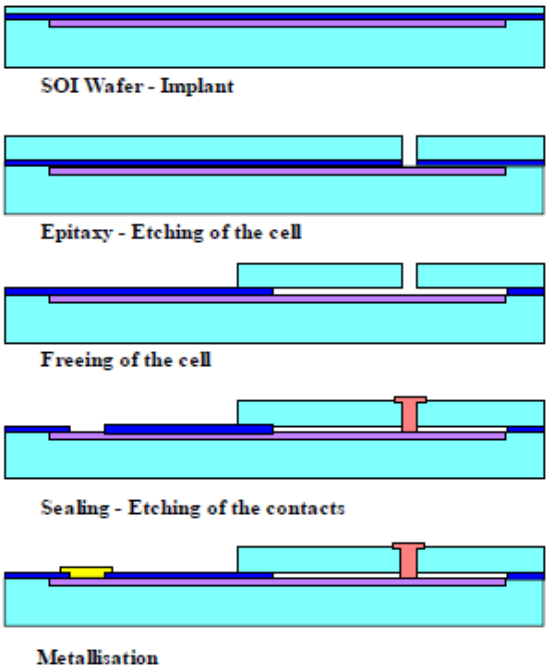

Figure 18 - Tronics Pressure Sensor Fabrication Process [34]

As mentioned earlier, the simple process makes very small highly sensitive pressure sensors targeting the implantable pressure sensor market. There are two major problems with the fabrication process. The first is the control and reproducibility of the etch cavity. Since this etch is within the cavity it is very difficult to monitor. Effects can be reduced by properly controlling the etchant parameters, however variability is almost inevitable. Another issue is with the dielectric sealing mechanism [8]. Degradation of the vacuum reference has been shown in long term applications, leading to signal drift due to increasing reference pressures [8]. This method also complicates the mechanical loading mechanism as the circular membrane is now fixed at the center of the membrane as well as its circumference [21].

In terms of the design process, an important factor that must be accounted is signal noise due to changes in temperature. Temperature dependence of the sensor is mainly due to the parasitic capacitance of the entire device. Temperature compensation in the CMOS circuitry can be used to offset this dependence. However, a more effective method is to do a differential measurement with a rigid reference sensor of similar dimensions [34, 35]. A reference sensor can be made simply by not etching the cavity or inserting several plugs into the membrane. The result is that parasitic capacitance is considered a common mode load on the system and cancelled by a differential measurement which would need a less complex compensation circuit [34].

Bosch Sensortech

BMP180

One of Bosch Sensortech's most promising technologies is advanced porous silicon membrane (APSM) process [8]. First introduced in 2003, APSM is a surface micromachining technology for fabricating single crystal silicon membranes covering a vacuum cavity [36]. The technique offers the mechanical advantages of bulk micromachining with the CMOS compatibility of surface micromachining. The main process steps are: (i) local anodic etching of layered porous silicon with different porosities, (ii) thermal rearrangement of the porous silicon and (iii) epitaxial growth of the silicon membrane layer.

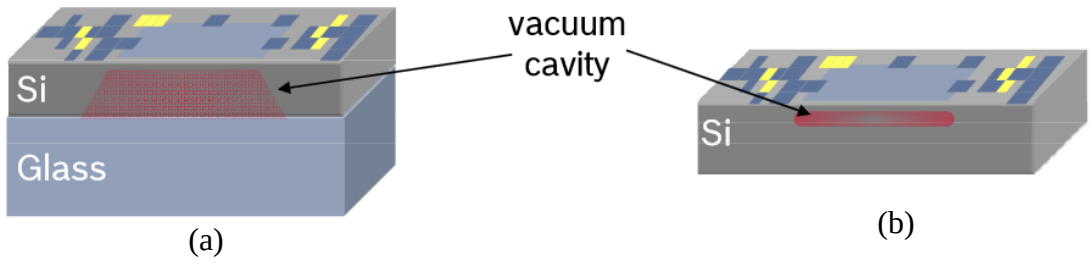

Figure 19 - Traditional Wafer Bonded Pressure Sensor (a) and APSM Pressure Sensor (b)

The process begins with a p doped wafer <100> wafer. Shallow p+ doped and deep N+ doped regions are made on the front side of the wafer while the backside is p doped to improve the conductivity of the wafer. Silicon nitride is used as the etch mask to protect the N+ doped regions and expose the p+ to HF [36]. The anodic etching is carried out in two steps to vary the porosifaction between the P+ doped shallow membrane region and the buried region which will

become the cavity. The details of the silicon porosification in HF are described by Lehman [37]. The mask is removed and the device undergoes an annealing process at elevated temperatures in a CVD hydrogen rich atmosphere. The hydrogen is used to dissolve the oxide allowing the silicon to rearrange and form one large cavity. After the prebake, the temperature is raised to 1100C for epitaxial growth using chlorosilane setting the membrane thickness and hermetically sealing the pressure reference [8, 36].

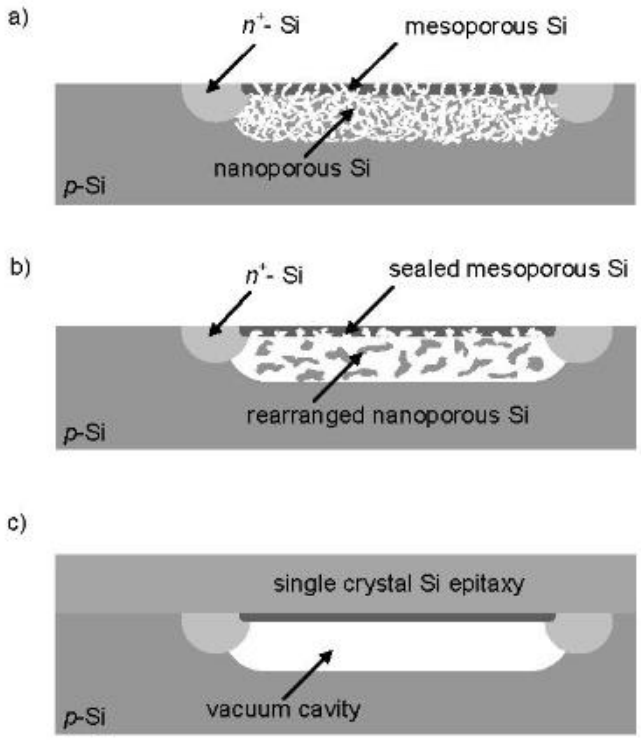

Figure 20- Bosch Sensortech's APSM fabrication process [36]

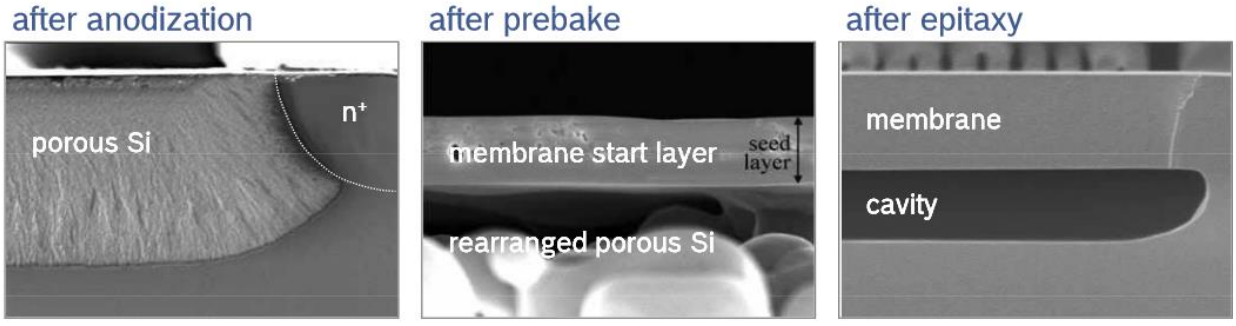

Figure 21- Crossectional View of Pressure sensor at different fabrication steps [36]

The wafer is ready to undergo CMOS steps to seamlessly integrate the ASIC on a single dye. This process has been commercialized under Bosch Sensortech's BMP180. This technology represents Bosch's smallest pressure sensor to date [36]. The BMP180 is a low cost full wheatstone bridge piezoresistive device geared for the smartphone and wearable market to assist GPS location technologies [33, 36, 37].

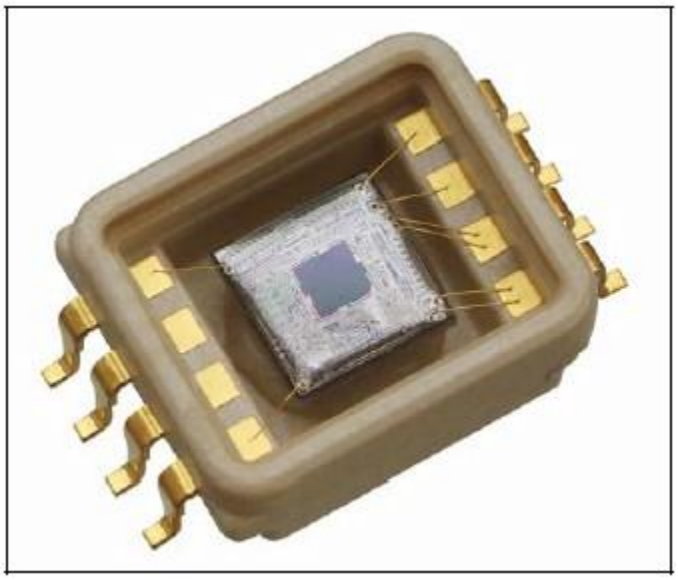

Figure 22- Packaged Sensor with integrated CMOS from Bosch Sensortech [36]

APSM Capacitive Pressure Sensor

In 2009 a capacitive pressure sensor was developed using the APSM process [30]. Expanding this technology to capacitive transduction allows for greater flexibility in tailoring the sensor properties to specific applications. This is achieved by adding a poly silicon fixed electrode above the membrane during the CMOS implementation [30]. This process provides a single crystal silicon pressure sensitive membrane taking advantage of its unique properties like high strength, high reliability and no mechanical hysteresis. Second, the process is CMOS compatible. Third, since the dimensions of the electrodes are confined by an etch trench and the electrodes are isolated by a dielectric layer it has stable temperature behavior [30]. To reduce the effects of parasitic capacitance, a reference capacitor is placed with a non-deformable membrane. An integrated differential capacitive to digital convertor is used to measure the capacitive signal [30, 33, 36].

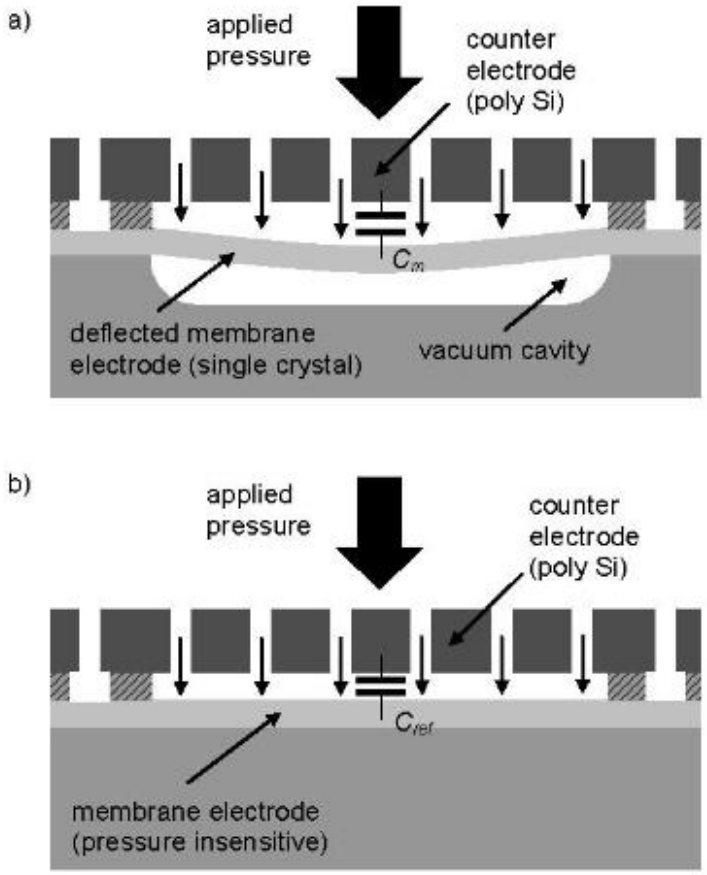

Figure 23- Parallel Capacitive Pressure Sensor with APSM process [30]

The APSM process was described earlier in this section when describing the BMP180. A 1um silicon oxide film is deposited on the APSM wafer, which will serve as the dielectric and electrode gap. The silicon oxide is patterned then a thick 10um layer of polysilicon is deposited on the wafer in a CVD reactor. Access holes are etched into the membrane region using DRIE to reveal the buried oxide layer. The silicon oxide is etched using HF vapor releasing the fixed polysilicon electrode [30, 36].

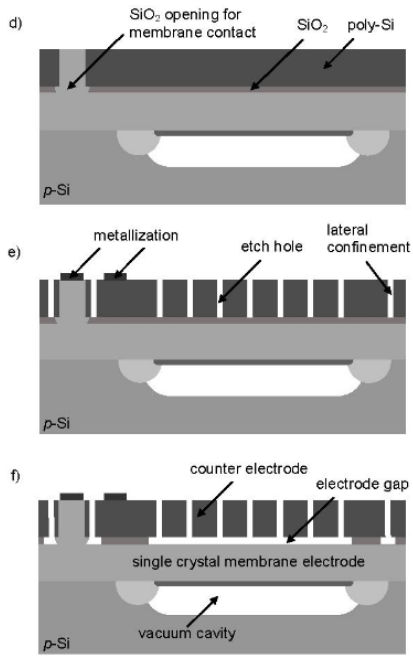

Figure 24- Fabrication Method for a capacitive Pressure Sensor using APSM process [30]

However, with this electrode arrangement, the membrane will deflect away from the fixed electrode. This act will diminish the signal strength rather than increase it like in a typical parallel plate implementation. Also, since the membrane is free to deflect, the surface will most likely be non-planar during the poly-silicon deposition step [30]. This can cause non-linearity and batch reliability problems that will limit the performance ranges that can be achieved with this process [30].

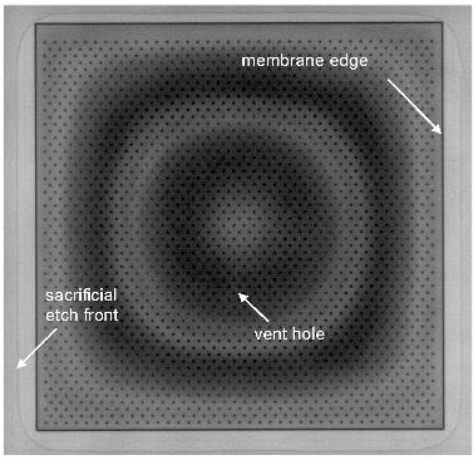

Figure 25 - Conformal Circles caused by deflected membrane during Polysilicon Deposition [30]

Proposed MEMS Capacitive Pressure Sensor

The MEMS Integrated Design for Inertial Sensors (MIDIS) process which was recently introduced by Teledyne DALSA Semiconductor Inc. (TDSI) offers a pure-play mass-production platform to make high performance MEMS inertial sensors including gyroscopes and accelerometers [2, 38]. In most motion sensing applications, gyroscopes and accelerometers have been combined with their associated circuitry to create 6-axis (3-axis gyroscope and 3-axis accelerometer) inertial measurement units (IMUs) [4]. These IMUs have been recently combined with 3-axis magnetometers to create 9-axis IMU systems. One of the most commercially successful devices are the IMUs developed by Invensense Inc. The information that is missing from these IMUs is an absolute reference of altitude position in space. The goal of this project is to create a series of post processing steps compatible with the MIDIS^{TM} platform process to create integrated absolute referenced pressure sensors. Our process will takes advantage of the high, clean vacuum and low leak rate of 45 molecules/s ($7.5E^{-13}$ atm·cc/s) which is several orders of magnitude better than Military-Standard 883H ($1E^{-9}$ atm·cc/s or 61,500 molecules/s) that is commonly accepted by industry [2, 3]. A stable reference is critical for high accuracy non drifting pressure sensing. Our process also allows for integration of 3-axis accelerometers, 3-axis gyroscopes along with a pressure sensor to be monolithically integrated on a single die. This system combined with a 3-axis magnetometer (available as a standalone chip) opens the door for the world's smallest, lowest power and highest performance fully integrated 10-axis IMU. This technology will enable the next generation products in inertial motion tracking technology [2, 38-41]. Our process also takes advantage of the high, clean vacuum and low leak rate of 45 molecules/s ($7.5E^{-13}$ atm·cc/s) which is several orders of magnitude better than Military-Standard 883H ($1E^{-9}$ atm·cc/s or 61,500 molecules/s) that is commonly accepted by industry [2, 3].

MIDIS^{TM} platform

The MIDIS^{TM} platform introduced by TDSI is a pure-play silicon micromachining process platform designed for inertial sensor applications. The MIDIS^{TM} platform includes one single-crystal silicon device wafer that is vacuum encapsulated between two other fusion bonded silicon wafers, a handle wafer and an interconnect wafer. Through-Silicon Vias (TSVs) are used to make electrically isolated connections to the device wafer [39]. This process is characterized by a thick bulk single crystal silicon device layer, high quality hermetic wafer level packaging (WLP) and flip chip compatibility [2].

The process begins by patterning the bottom wafer (known as the handle wafer) and expose it to a deep silicon dry etch [39]. The deep silicon dry etch process used involves four distinct steps patented by TDSI. The first is deposition of a protective polymer on a patterned substrate. Followed by a low pressure (less than 40mTorr) etch to partially remove the deposited polymer. Then a high pressure etch (between 40-1000mTorr) to form a portion of a trench in the substrate. At this point these steps resemble a Bosch process. The difference is in the final step where a second low pressure etch (less than 40mTorr) is performed [39]. This final step helps to fabricate deep trenches with reduced surface roughness. These four steps are repeated in sequence until the desired depth profile is reached.

In MIDIS^{TM} platform, the Deep Reactive Ion Etching (DRIE) process is used to create 30um deep silicon cavities (b) in the handle wafer [39]. The surface is then protected by a 1.1um thermally grown layer of silicon oxide (c). The silicon oxide is used to protect the bottom wafer during further processing. The next step is fusion bonding the 30um (100) silicon device layer onto the handle wafer. To facilitate this process, the 30um Device layer is placed on its own handling wafer in a Silicon on Insulator (SOI) like configuration. Heat and pressure are applied to fuse the device wafer to the handle wafer. The 30um device layer is then isolated from its wafer using Chemical Mechanical Polishing (CMP) and SiO_2 etching (d).

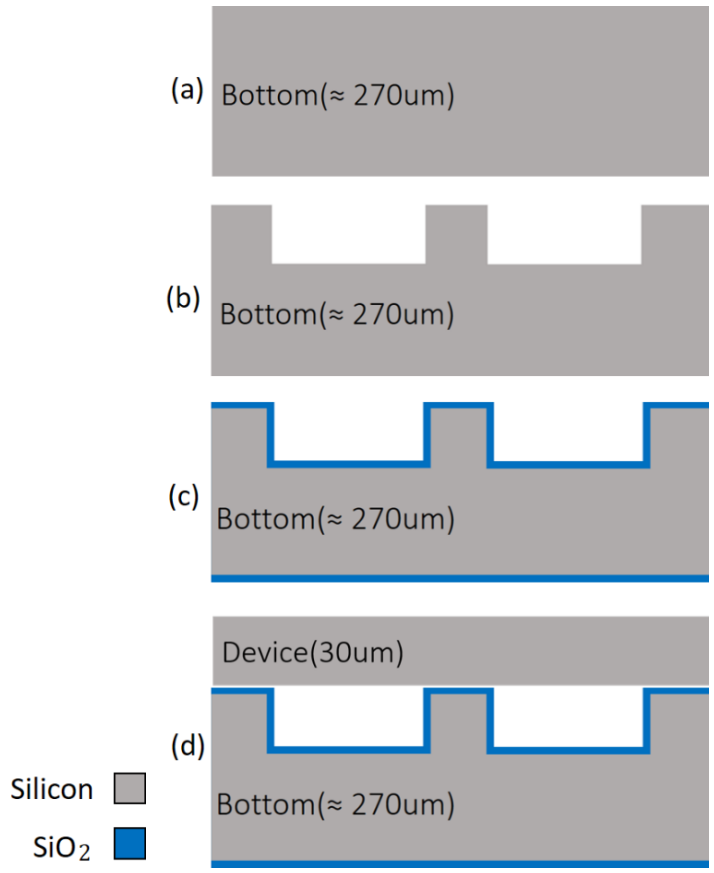

Figure 26 - Bottom Carrier Wafer Process Steps (a-c). With Bonding of Device Layer (d)

The device layer is patterned in order to prepare the layer for a DRIE step. The features are aligned over the bottom wafer cavities by use of markings on the backside. The DRIE etch step etches through the 30um device layer releasing the structures. This step is also used to electrically isolate the structures within the device layer (e). This DRIE etch step is typically preformed with a Bosch process using SF_6 as the etchant and a Teflon like polymer to protect the side walls and create vertical profiles. The 1.1um thermal oxide layer on the bottom handle wafer is used as an etch stop for this DRIE step [39]. The following step involves patterning these isolated structures. This is done typically by spray coating the surface and photo patterning the structures that will be etched. Alignment is a critical part of this step in order to have a uniform etch (e). The 4um etch is important for electrostatic comb drive structures at it allows for the fixed electrodes to be smaller than the moving electrodes [40]. During actuation, the reduced thickness of the fixed comb fingers can be used to reduce or prevent the formation of fringe electric fields at the top and bottom portions of the comb fingers, which can cause the comb fingers to move out-of-plane under certain circumstances [40].

Figure 27 - Cross Section of the Device Layer Etch Step. This is where the devices geometry is made. Left is the accelerometer, right is the isolated pressure sensor. This method enables patterning without having to release the structures eliminating the need for etch holes and allowing thick device layers. The second etch step allows for reduction in fringe effects and cross sensitivity issues by eliminating the risk of comb overlap.

In parallel, the top wafer has undergone its own set of bulk micromachining steps in order to prepare the top wafer for fusion bonding with the device wafer shown in Figure 28. The top interconnect wafer is etched on the bond side and then processed from the top of the wafer (b). The first step in the processing of the top wafer is to properly identify and protect the bonding plane of the wafer. Surface area, material composition and surface quality are integral to a strong uniform fusion bond. In MIDIS^{TM} platform, the bonding plane is isolated by placing a protective layer and performing a 2um anisotropic wet etch of the exposed silicon wafer. The 2um etch could also be possible with TDSI's 60^{o} anisotropic dry etch. This separates the rest of the processing steps from the bonding plane.

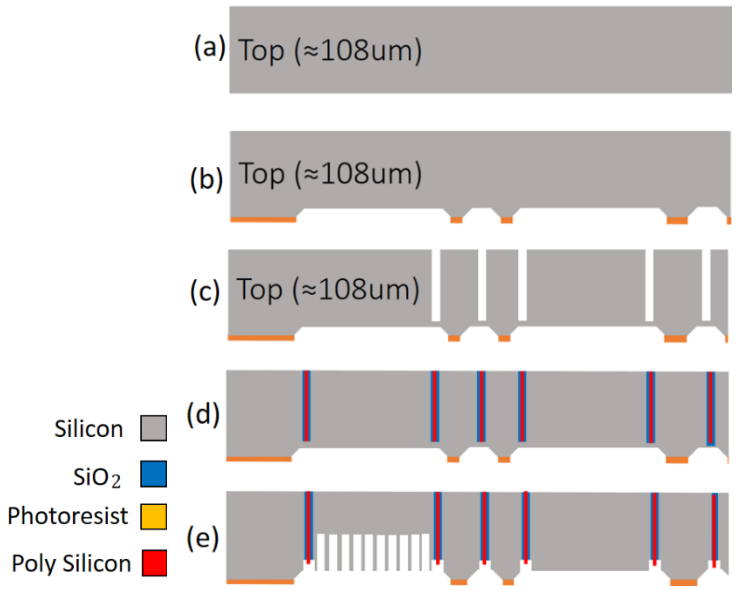

Figure 28 - Top wafer Processing steps are done in parallel with the Bottom wafer. The photoresist on the bond plane is critical to the bonding of the wafers after being processed.

The next step is creating the Through Silicon Vias (TSVs). TSVs are integral to the design and functionality of hermetically sealed MEMS devices as they allow for the electrical connection of isolated structures within the encapsulated device (c). The channels necessary for TSVs are etched using a DRIE like process. Similar to the device wafer etch step, the TSV etch creates vertical walls that travel through the bulk silicon in the top wafer (108 um thickness). This step electrically isolates the bulk wafer and prepares the top wafer for the creation of TSVs. Further deposition steps are performed on the top side of the wafer. Before these deposition steps, a final DRIE step is used to create a larger cavity in the top wafer (e). This DRIE process is similar to the backside cavity etch outlined above [39]. After this etch, the bond side patterning profile is complete and top wafer is flipped to work on the final steps before bonding (f).

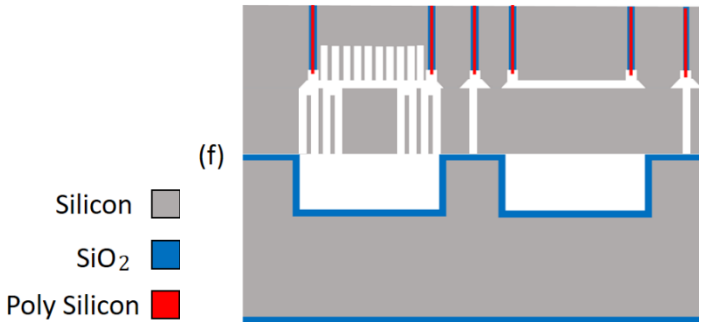

Figure 29- Cross Section of MIDIS Process after Top Wafer is bonded to the Device layer and bottom carrier wafer. This is a critical step as the heat and processing will determine the quality of the vacuum.

The machining steps on the topside of the top wafer are characterized mostly by surface micromachining. The first deposition is a 1 um layer of silicon dioxide using PECVD using acqueous tetraethoxysilance (TEOS) (f). This deposition method helps coat the top side and within the channels of the TSVs. Serving as a dielectric material for electrical isolation. The second step is to deposit 2um of phosphorus doped polysilicon using LPCVD. This highly N-type polysilicon along with the oxide dielectric are used to create an electrical barrier within the TSV channels isolating the conductive elements within the device. The top wafer then undergoes a CMP process that removes the top coat of polysilicon leaving only what is present in the channel (f). Finally, metal pads are electroplated onto the wafer and isolated using both PECVD TEOS SiO_2 and a polymer film [2, 38-41].

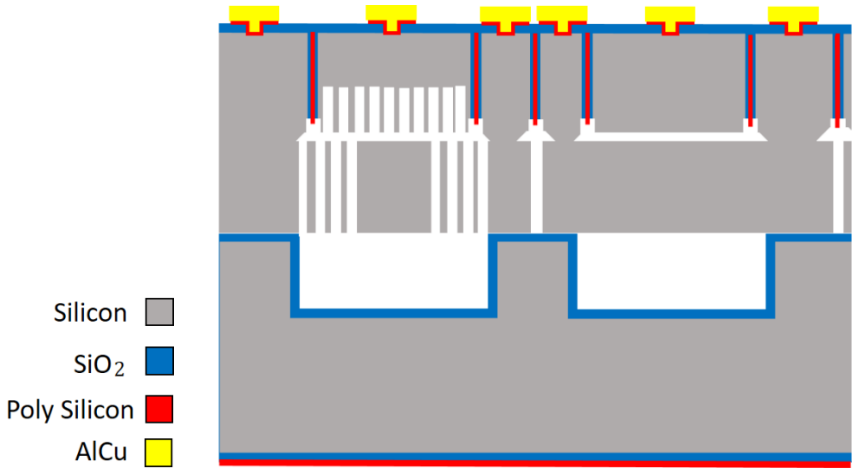

Figure 30 - Cross Section of the MIDIS™ platform with Accelerometer on left and Pressure Sensor on right before Post Processing.

Post Processing Steps: Development of the MEMS Pressure Sensor

As stated above, the post processing steps must be compatible with the MIDIS™ platform and enable the integration of multiple MEMS devices on a single die. This process necessitated a method to expose the encapsulated membrane, while leaving the other structures encapsulated. From the two possible micro-machining methods (dry etch or wet etch) available to perform this step, DRIE in a Bosch style process was chosen, as it enabled the isolated etching of the bottom cavity without exposing the other devices on the wafer. Also, dry etching of the handle wafer allows for protection of the topside metal connections, which is not possible with a wet etching approach. Finally, the vertical anisotropic sidewalls of a Bosch process limits the amount of area

wasted by the channel formation creating the smallest possible footprint for a pressure sensor in the MIDIS^{TM} platform.

Before etching the handle wafer, the bottom side of the wafer had to be properly prepared. The wafer had a layer of 0.3um polysilicon deposited via LPCVD as a seed layer for the AlCu bond pads on the top wafer. This also coated the bottom of the handle wafer and need to be etched. A 2:30 min Reactive Ion etching (RIE) step was used to process the polysilicon. Sulfur hexafluoride (SF_6) is used as the etching gas, which creates a plasma of fluorine radical ions that create volatile silicon compounds when contacting the surface of the chip quickly removing the polysilicon layer. Perfluorcyclobutane (C_4F_8) is organic gas that improves the etch quality of the chip by protecting the side walls from SF_6 etching similarly to a Bosch Process, but at reduced etch rates.

Table 3 - Polysilicon Etch Recipe

Temperature	Duration	Gas	Power
15 C	2:30 min	19 sccm SF6 20 sccm C4F8	1500W ICP 50W RF

Figure 31- Cross Section of MIDIS^{TM} after Polysilicon Etch. An etch mask is used to only etch the area above the pressure sensor. The mask is aligned using features on either the top or bottom wafer.

The polysilicon etch step exposes the underlying 1.1um thermal oxide that was grown during one of the early process steps of the handle wafer to protect the bottom cavity during the structural deep etching of the device layer. This SiO_2 (known as silica) can be removed using an RIE etch of tetrafluoromethane (CF_4). The CF_4 creates a plasma of fluorine radical ions that combine with

silicon to produce volatile compounds while the carbon atoms combine with the oxygen atoms to form volatile carbon dioxide and keeping the oxygen atoms from reacting with the underlying silicon. Helium is used to improve the amount of gas collisions within the chamber lowering the amount of energy needed to ignite the plasma. Helium also acts like a carrier to transport the volatile compounds out of the etching chamber.

Table 4 – SiO_2 Etch Recipe

Temperature	Duration	Gas	Power
25 C	8 min	50 sccm CF4 50 sccm He	2750W ICP 100W RF

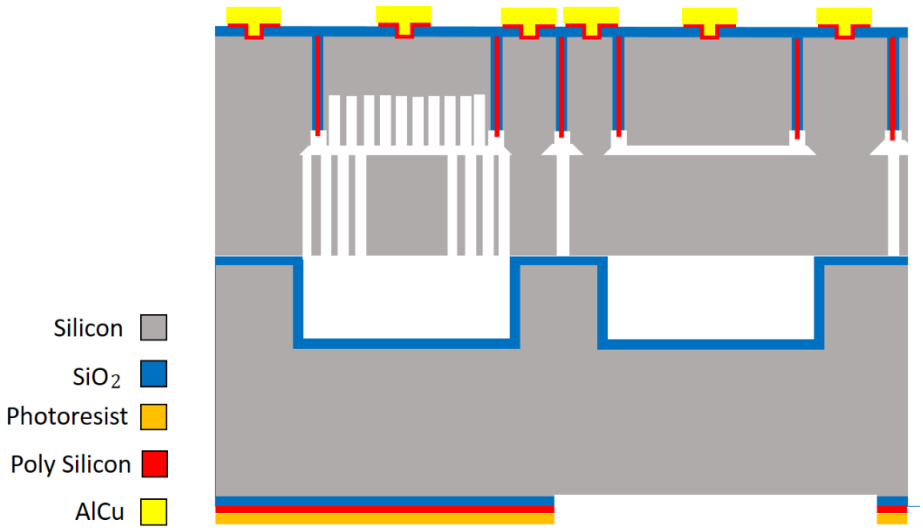

Figure 32- Cross Section of MIDIS™ after SiO_2 Etch. Notice that only the Silicon above the Pressure Sensor is exposed. The Accelerometer is protected to ensure both devices can be made on a single die.

Following these two RIE etch steps, the handle wafer is ready for the deep etch to expose the device wafer. This etch is done using a Bosch process with alternating polymer deposition and fluorine etch steps. The parameters were tuned to improve etch rate while keeping the side walls as vertical as possible, side wall scalloping was deemed important. This process is called the long exposure high RF power (LEHP) etch. The LEHP etch is carried out in alternating steps until the bottom cavity is reached. The SiO_2 layer above the bottom cavity acts like an etch stop protecting the device layer from this deep etch process. The duration of this LEHP etch is 1hr 30min.

Table 5 - LEHP Etch Recipe

Temperature	Duration	Gas	Power
15 C	8 sec	500 sccm SF6	3000W ICP 50W RF
15 C	3 sec	450 sccm C4F8	3000W ICP 0W RF

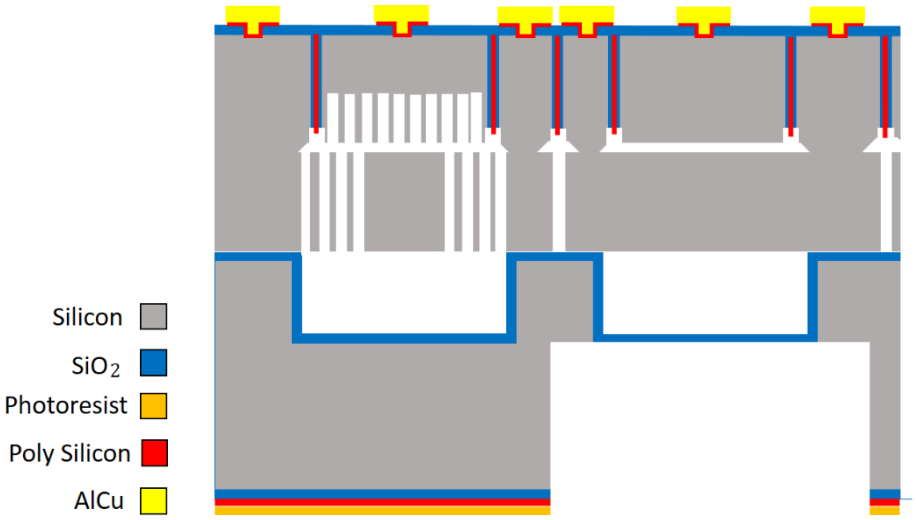

Figure 33 - Cross Section of MIDIS™ after LEHP Etch. The oxide layer is exposed and acts like an etch mask which reduces the control parameters on the LEHP Etch step.

Once this etch is complete, the channels have been created within the handle wafer and the SiO_2 layer above the bottom cavity must be removed to expose the device layer for the diaphragm etch step. The same SiO_2 etch is used for this step. Special attention is placed on the duration of the step in order to ensure no oxide remains within the bottom cavity. This special attention is done because these silica particles can act like etch masks, which may cause imperfections in the following diaphragm etch step.

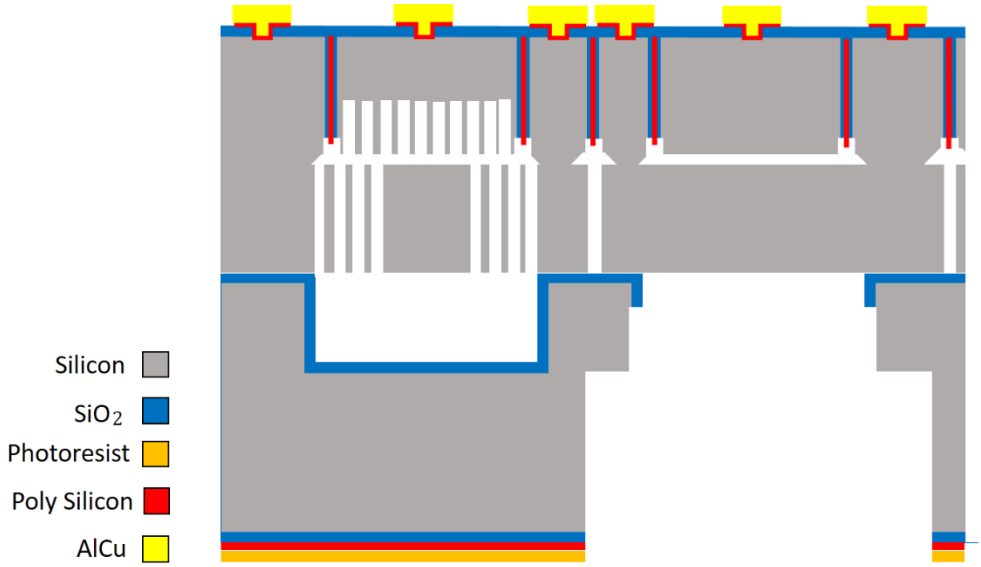

Figure 34 - Cross Section of MIDIS™ after SiO_2 Etch exposing the device layer to the most critical step in the process. The SiO_2 is ran long to ensure no SiO_2 is left on the Device layer which would act like an etch mask.

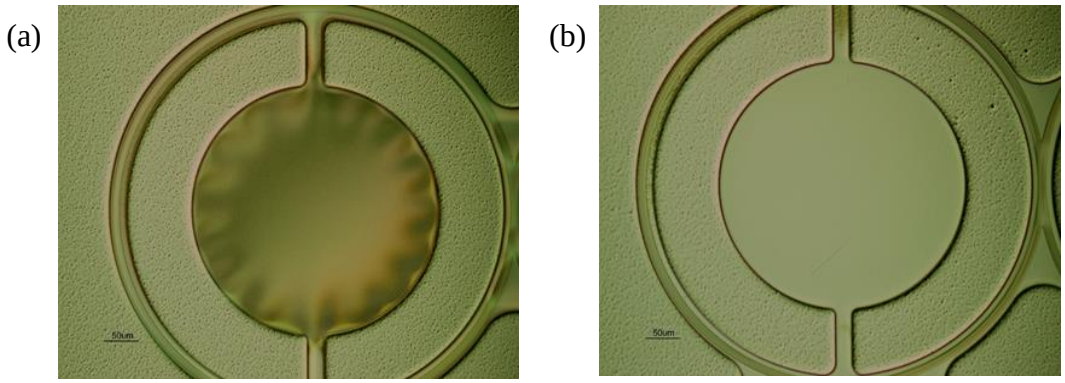

Figure 35 - Top View Before (a) and After (b) Etch. Notice the concave deflection of the SiO_2 layer demonstrating the vacuum within the bottom cavity that creates a pressure gradient under atmospheric conditions.

The final step is one of the most critical steps in this post-fabrication process. It is critical because the etch duration will determine the thickness of the silicon membrane. The thickness has a direct effect on the rigidity and ultimately the performance of the pressure sensor. Typically, this step is controlled via a well-controlled wet etching process. However, due to the crystallographic characteristics of this wet etch, the membrane performance would need to be determined based on the geometry of the bottom cavity. This fact limits the versatility of the design. Another problem is that wet etchants at scale would most likely affect the topside layers of the chip reducing its compatibility with the MIDIS™ platform. For these reasons, a Bosch process was chosen. The parameters were tuned to improve surface quality and reduce the amount of material etched per step. This process is known as the short exposure low RF power (SELP) etch. Preliminary tests

were run to find the precise etch rate per step. From there the number of steps were set to control the thickness of the membrane.

Table 6 - SELP Etch Recipe

Temperature	Duration	Gas	Power
15 C	4 sec	500 sccm SF6	3000W ICP 25W RF
15 C	2 sec	450 sccm C4F8	3000W ICP 5W RF

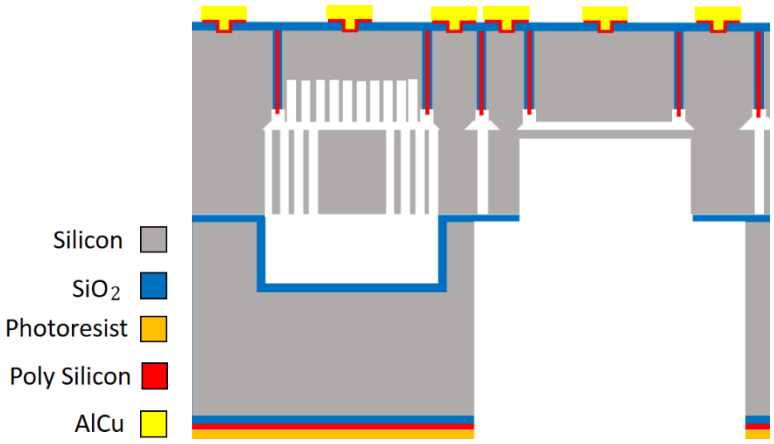

Figure 36 - Cross Section of MIDIS™ after SELP Etch. This is the final cross section of the pressure sensor. The number of etch steps determines the thickness of the membrane (device layer). This is the most critical step in the process.

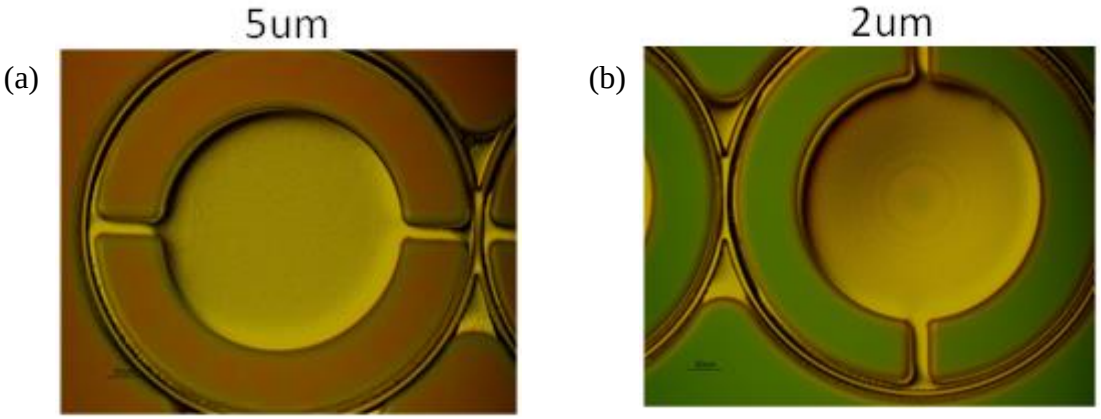

Figure 37 - Top View of Membrane after SELP etch for 56 etch steps (a) and 63 etch steps (b). Concentric circles on the membrane of (b) shows that it is deflecting towards the bottom electrode under atmospheric conditions.

These changes improved the controllability of the etching process and allow for single step variations in mechanical performance of the pressure sensor. The proposed method of manufacturing pressure sensors allows the ability to make application specific devices economically, reliably and with low lead times [42].

From Die Level to Commercial Scale

It is one thing to make something in the controlled confines of a lab, it's another thing to repeat it on a commercial scale. Since the post processing steps were developed to be compatible with a high throughput commercial process studying the scalability of this post process will help increasing the value of this work. From the process detailed above, the most difficult step to run commercially is the thickness control etch. The problem is repeatability and uniformity over the entire wafer. Typically, DRIE etch steps results in uniformity issues due to a higher concentration of ions on the periphery. The higher concentration of radical ions is caused by the lower consumption of radicals from the cathode electrode supporting the substrate. This results in a phenomenon known as the bull's eye effect named after the circular patterns that are formed. This effect can be reduced by making the cathode material consumable at the same rate as the wafer. However, consuming the cathode will lead to more maintenance complications. Another method would be to design the wafer such that different devices on the periphery are tuned for this larger etch rate. A wafer level study is needed to show the actual difference in etch rate throughout the wafer diameter. From this study, we would have a more accurate representation of the yield of the wafer given a fixed design.

Another aspect that should be considered is wafer level CMOS bonding. In order for this process to be successful, accurate dimensions of pad locations and important features would need to be perfectly aligned. The bond pads would also need to be distributed on the four corners of the device. This is important to ensure a strong bond between the CMOS circuitry and MEMS device especially during wafer dicing steps. If the MEMS components are not uniformly supported, it could lead to connection problems which would affect the yield and subsequently the cost of these devices [42].

Design

The Goal

The main goal of this project was to develop a method to make pressure sensors within the MIDIS^{TM} platform. Comparing to current state-of-the art, the developed pressure sensors should be the smallest, lowest power and highest performing sensors. From the MIDIS^{TM} platform, two main pressure sensing mechanisms were identified. The first was diaphragm based capacitive device made from the device layer with a vacuum reference pressure. The second is a vacuum encapsulated resonant frequency based device where the pressure transfer would take place at the bottom cavity's thermally grown silicon dioxide layer. From the start, both sensing methods seemed promising. However, the diaphragm based capacitive mechanism was chosen due to the simplicity of the sensing mechanism, availability of signal processing CMOS chip and relatively lower power consumption.

Once the mechanism was identified the next step was to identify which applications we should target. To showcase the versatility of this fabrication process, three different applications were identified in biomedical, environmental, and energy extraction applications. The pressure sensing requirements are listed below.

Table 7 - Application Requirements of pressure range and resolution.

Applications	Min Pressure	Max Pressure	Resolution
Biomedical	50kPa	130kPa	0.2kPa
Environmental	111kPa (1m deep)	352kPa (25m deep)	0.8kPa (5cm)
Energy Extraction	111kPa (1m deep)	1106kPa (100m deep)	2kPa (20cm)

From these requirements, the membrane's dimensions should be chosen. The MIDIS^{TM} platform allowed for freedom in both the x and y plane (perpendicular to applied pressure) and the post processing thickness control etch allowed for freedom of the membrane thickness. The membrane had a maximum thickness of 30um as this is the thickness of the device layer. A minimum thickness of 1um was chosen as a limitation of the thickness control etch due to the increased etch

rate at the periphery of the device (Bull's eye effect). Another limitation is the distance between the membrane and the bottom fixed electrode, also known as the gap. In the MIDIS^{TM} platform, the gap distance could be 2, 6, 20 or 26um. Since capacitance was chosen as the transduction mechanism, minimizing the gap maximizes the signal and improve the transduction efficiency. For this reason, a 2um gap was chosen.

From a design standpoint two other factors that must be considered are the material properties of the membrane as this will limit the performance of the sensor. Another important aspect that is typically overlooked is the measurement limitations imposed by the capacitance to digital CMOS circuitry. Considering the electrical limitations helps to optimize the sensors performance to suit a particular application.

Designing around the IC

Today, the wide scale popularity of touch screen devices has led to a large influx of high performance commercially available capacitive-to-digital convertors (CDC). Two CDCs were chosen that fit the criteria for our intended applications.

Analog Devices: AD7152

The AD7152 is a 12-bit sigma-delta CDC. The capacitive transducer can be directly connected to the inputs. The architecture features very high resolution down to 0.25fF and high linearity (±0.05%). This product contains four different operating modes, ±0.25pF to ±2pF in differential mode and 0.5pF to 4pF in single ended mode designed for floating capacitive sensors. The AD7152 will accept up to 5pF in common-mode capacitance which can be balanced using on-chip, digital-to-capacitance converters.

The AD7152 has a 2-wire, I^2C compatible serial interface. The CDC operates with a single power supply from 2.7V to 3.6V consuming 100µA. It can function over a temperature range of -40^{o}C to +85^{o}C.

Micro Analog Systems: MAS6512

The MAS6512 is a 16-bit sigma-delta CDC. The capacitive transducer can be directly connected to the inputs. The architecture features very high resolution down to 0.022aF. The MAS6512 has three different operating ranges from 0-1.8pF, 0-4pF and 0-20pF in both difference mode and ratio mode. The convertor will accept up to 22pF in common-mode capacitance which is balanced using on-chip, digital-to-capacitance converters.

The MAS6512 is 2-wire I^2C and 4-wire SPI compatible serial interface. The CDC operates with a single power supply from 3.6 to as low as 1.8V consuming very little current (between 3.3 and 24.1µA). It functions over a temperature range of -40^{o}C to +85^{o}C.

From these brief product descriptions it is easy to see the benefit of using the Micro Analog Systems MAS6512. The MAS6512 has advantages of lower operating voltage, lower power consumption, larger common-mode capacitance offset, larger dynamic range and an order of magnitude higher resolution. From a manufacturing point of view, the MAS6512 also has the advantage of being available in both wafer and bare die format. This feature allows for smaller dye level packaging formats.

From a design perspective, it is important to have a large dynamic range with high resolution. This ultimately will determine the limitations of the sensor performance. Another important feature of the MAS6512 is that it has the ability to offset up to 22pF of common-mode capacitance. Large offset capacitance allows more freedom with the design enabling smaller diaphragms rather than a few larger diaphragms. Given the configuration of these pressure sensors in the MIDIS^{TM} platform, much of the capacitance signal is created between the bulk of the fixed electrode and the channel of bulk silicon needed to reach the sensing diaphragm as shown in Figure 34 below. This steady-state capacitance is a function of the surface area between these two structures. Decreasing the membrane dimensions leads to more diaphragms needed for a given signal and therefore a larger surface area of non-varying capacitance. Since smaller diaphragms allow for thinner membranes and a quicker response time. Larger offset capacitance also allows for more freedom of how the pressure sensors are arranged enabling the canceling of common mode sources of capacitance. There are also other forms of parasitic capacitance that lead to common mode noise within the signal. These sources include bond pads and parallel circuit lines. A large offset capacitance eliminates these sources from the actual signal making for a more accurate response.

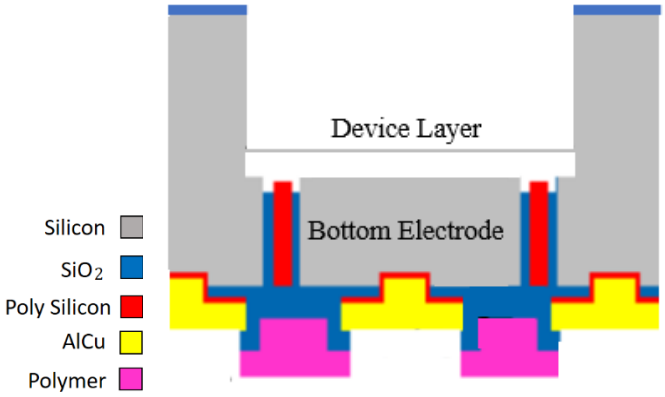

Figure 38 - Capacitive Pressure Sensor in MIDIS™. The thickness of the device layer controls the pressure range and sensitivity of the sensor. The reference pressure between the device layer and the bottom electrode is vacuum.

Picking the Dimensions

A sensor's mechanical performance is based on deflection of the membrane, center deflection, strain energy and resonance frequency. For isotropic materials, static deflection can be solved using *Kirchhoff-Love Plate Theory. [26]* Assuming a mid-surface plane can be used to represent a three dimensional plate in two-dimensions as given by Equation (16),

$$\frac{\partial^4 w}{\partial x^4} + 2\frac{\partial^4 w}{\partial x^2 \partial y^2} + \frac{\partial^4 w}{\partial y^4} = \frac{p}{D_i} \quad (16)$$

where p is the applied pressure difference across the plate and the isotropic rigidity, D_i, and is given by Equation (17),

$$D_i = \frac{E\mathrm{h}^3}{[12(1-\nu^2)]} \quad (17)$$

where E is the Young's modulus, ν is the Poisson's ratio, and h is the thickness of the plate. The plate equation is then solved using the clamped boundary conditions and the obtained deflection surface can be used to calculate the capacitance of the device. For circular plates, it is convenient to use cylindrical coordinates [26]. The static deflection $w(r)$ with radius, a, clamped at the circumference is given by Equation (18) as,

$$w(r) = w_0\left[1 - \left(\frac{r}{a}\right)^2\right]^2 \quad (18)$$

Assuming clamped boundary conditions the center deflection is given by Equation (19),

$$w_0 = w(0) = \frac{pa^4}{64D_i} \quad (19)$$

These expressions are only valid for thin plates (i.e. aspect ratio $a/\mathrm{h} \geq 40$) with small deflections compared to the thickness of the plate (i.e. $\mathrm{h}/w \geq 5$) [26]. Since at these conditions, the stress stiffening effects can be ignored and shear deformation is small. Also, it is assumed that the plate is clamped at the boundary. In reality, these plates have elastic boundaries and can be compensated by increasing the effective radius of the plate. Finally, this analysis considers the material is isotropic. The problem is that silicon is an anisotropic material as shown in Table 8 [26].

Table 8 - Material Properties of Si in different orientations [9]

Silicon Direction	Fracture Toughness (MPa $m^{\frac{1}{2}}$)
<111>	0.83 to 0.95
<100>	0.91
<110>	0.94
Polycrystalline Silicon	0.94

Silicon with <100> orientation behaves strongly anisotropic and therefore the equations explained above do not properly explain the behavior of the system and can lead to 8-10% errors in calculation when compared to FEM simulations that take anisotropic conditions into account [26]. One popular method to correct for these errors is by taking a mean value of Poisson's ratio and Young's Modulus from all the crystal orientations [26]. This method reduces the error to about 1%. This approach has been well documented and is accepted in literature as the method to approximate the deflection of a thin plate [43]. Though flawed in its assumptions, the approach is simple and easy to implement. A more exact solution uses a derived plate equation that considers the crystal orientation of the silicon wafer. This model shows excellent agreement with anisotropic FEM calculations [26].

Since the mathematical models were only used to gain greater understanding of parametric effects, the mean value approach was preferred. From the model, increasing the diameter of the device has a, $w_0 \propto s^4$ effect on membrane deflection. While thickness has a, $w_0 \propto 1/s^3$ effect on the membrane deflection [25, 26].

The model was also used to gain a coarse idea of membrane dimensions that would be well suited for the three targeted applications. While this mathematical model helped focus the design, finite element modelling was essential to optimizing the pressure sensors.

Finite Element Analysis

One of the main drawbacks of finite element method (FEM) analysis is simulation time. Simulation time can be reduced by simplifying the model to its essential elements. Initially, all non-moving elements were removed from the mechanical model. A 2um support structure was added to the circumference of the membrane in order to accurately represent the boundary conditions. The mechanical structure was clamped at the bottom of the support structure, while the load was placed on the upper surface of the membrane. The mechanical model was used to fine tune the membrane's deflection, profile and resonance over a desired pressure range.

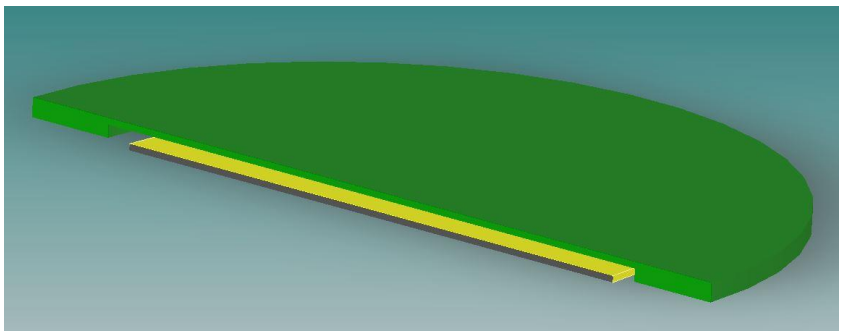

Figure 39 - Isometric View of FEM model Cross Section. The green section is the membrane, the yellow is the fixed electrode. The pressure is applied to the top of the green membrane causing deflection towards the fixed electrode.

A 1um fixed plate was placed 2um from the surface of the membrane to represent the bottom fixed electrode in the electrical model. The electrical model was coupled with the mechanical analysis to develop change in capacitance.

A second electrical model was developed that resembled more accurately the developed pressure sensors. This second model was used to get an idea of the parasitic capacitive loads and insure the values fell within acceptable ranges for current CMOS circuitry.

Figure 40- Cross sectional view of FEM model. The green section is the membrane, the black is the fixed electrode. The pressure is applied to the top of the green membrane causing deflection towards the fixed electrode.

These models were used to study the effects of diameter and membrane thickness on performance in both mechanical and electrical domains. The first analysis in Figure 41 shows membrane deflection with a fixed membrane thickness and with varying diameter.

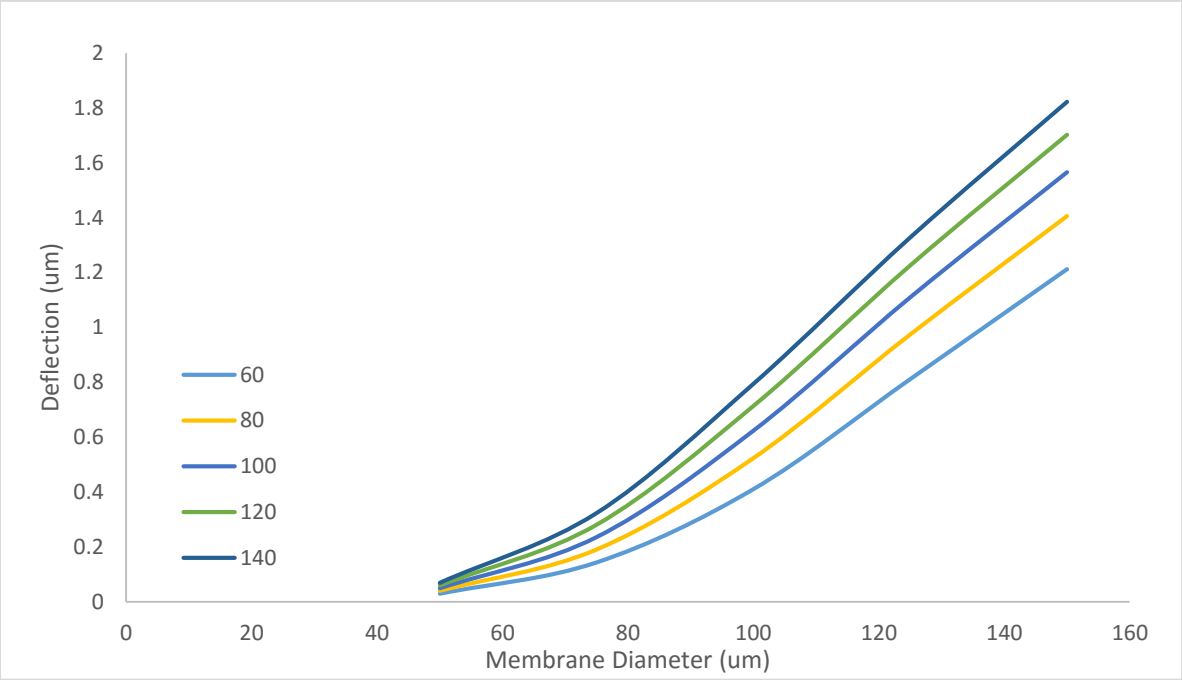

Figure 41 - Effect of Diameter on Membrane Deflection. As Membrane diameter increases, the deflection increases for a given pressure. Past 90um the change is linear with increasing slope based on applied pressure.

Figure 41 demonstrates the relationship between diameter and membrane deflection. The mathematical model in Equation (19) suggests the relationship as $w_0 \propto s^4$ with much steeper relationship than what can be seen in Figure 36. The variation can be explained by the introduction of internal stress within the membrane increasing the flexural rigidity (D). This term is difficult to quantify within the mathematical model as it requires considering anisotropic crystal structures.

The second analysis in Figure 42 observes the membrane deflection at a given diameter as a function of membrane thickness.

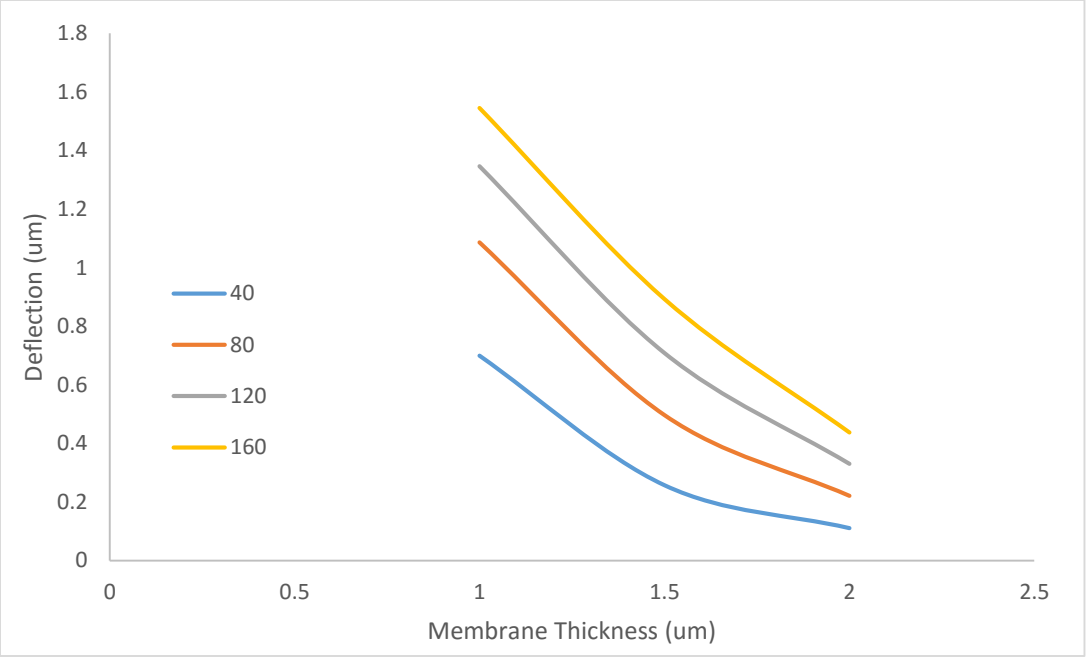

Figure 42- Effect of Membrane Thickness on Membrane Deflection as the thickness increases the deflection decreases. The effect is more noticeable with membranes of smaller radii.

Figure 42 demonstrates the relationship between membrane thickness and membrane deflection. The mathematical model in Equation (17) and (19) suggests the relationship as $w_0 \propto 1/s^3$. The current relationship has important implications for understanding how membrane thickness can be used to target specific pressure ranges.

Figures 41 and 42 are used to determine the mechanical performance of the membrane. This mechanical performance is transferred to the electrical domain by studying the change in capacitance.

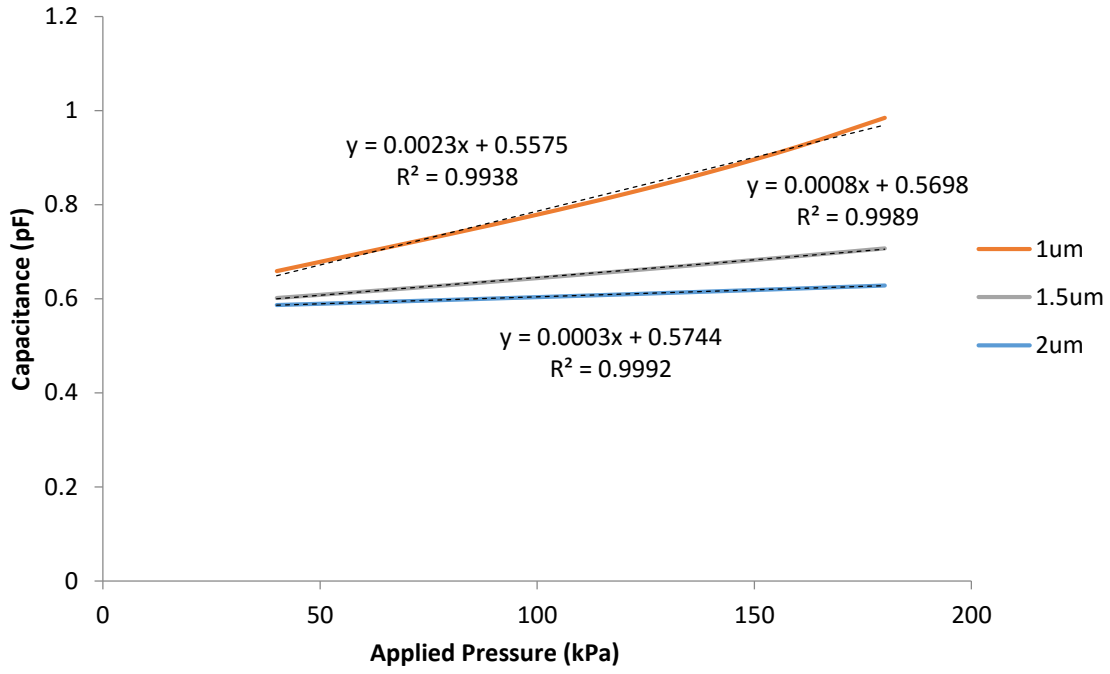

Figure 43 - Capacitance response of pressure sensors with varying membrane thickness keeping the diameter constant. The slope increases with decrease in membrane thickness.

Figure 43 demonstrates the relationship between capacitance readout and applied pressure. The relationship is used to optimize the capacitance readout over a given pressure range.

Table 9 - Summary of Simulation Results showcasing the effect of diameter and membrane thickness on Range and Resolution.

Diameter (um)	*105*		*130*		*150*		*180*	
Thickness (um)	3	5	3	5	3	5	3	5
Range (kPa)	1050	1050	750	1050	350	850	150	280
Range (pF)	0.325	0.137	1.583	0.716	0.669	1.054	0.883	0.879
Max Resolution (kPa)	0.073	0.220	0.015	0.044	0.013	0.031	0.004	0.009
Low Power Resolution (kPa)	0.833	2.500	0.167	0.500	0.147	0.357	0.044	0.104
Linearity (R^2)	0.991	0.998	0.958	0.992	0.953	0.981	0.953	0.984

Dynamic Modal Analysis

The dynamic performance of the pressure sensor was characterized. This analysis is important when subjecting the pressure sensor to vibrating loads. In order to mitigate adverse resonant noise in the signal, the first resonance frequency should be much larger than the frequency of the desire medium being measured. The analysis found the first modal frequency between 700-900 kHz depending on the dimensions of the pressure sensor. The second fundamental frequency was between 1.4 and 1.8 MHz. For the biomedical application, these resonant frequencies are much larger than the circulatory system of 1-1.67 Hz, and can be neglected. The resonant frequency can also be used to determine the frequency-response limit of the pressure sensor. The general rule of thumb is 20%, therefore the frequency-response limit is between 140 and 180 kHz [5].

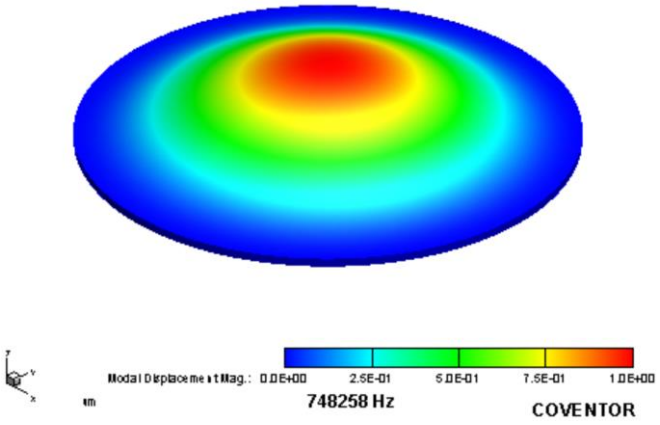

Figure 44 - First Mode of Pressure Sensor is at 748kHz

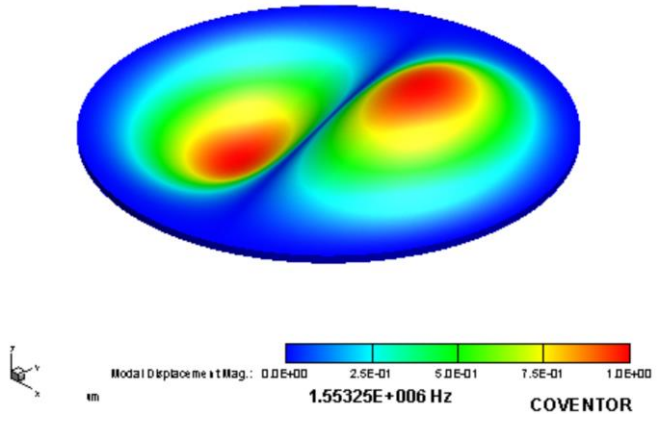

Figure 45 – Second Mode of Pressure Sensor is at 1.55 MHz

Testing

Characterizing the Fabrication Process

In order to properly characterize the fabrication process it is important to make quantitative and qualitative observations. Quantitative observations are especially important as a means of comparing between different process runs. This data can also be invaluable when optimizing steps within the process. The most important measures in microfabrication are etch rate, aspect ratio and selectivity. There are many methods to measure the etch rate, the most simple being total time needed to go through a layer of known thickness. While measuring time is simple, precisely identifying the moment when a structure has been etched is not without being able to continuously monitoring within the chamber. One method to dynamically identify a transition step is by measuring the surface refraction using a laser. Since refraction is a function of the surface properties, opacity and surface roughness, it can be used to measure large step changes like when a device transitions between silicon oxide and silicon or vice versa. Another method is by using a camera mounted to a glass window. This approach can be used to visually identify changes in surface features. This requires either periodic monitoring of the sample or video footage of the etching process. For the fast bottom cavity etch this method is very effective as the transition between the bottom wafer and the device layer is well defined.

A profilometer is typically used to measure surface roughness by laterally moving a stylus across a surface and measuring its height displacement. This method can be used to measure changes in height of a given sample with a known reference plane. This measurement is then compared with the etch time to get an average etch rate. Profilometers have the capability of measuring etch rates during a long bulk etch steps where the material properties do not change. However, removing the sample to make height measurements is tedious and imprecise. Contact based measurements are also limited by the performance and characteristics of the stylus making large step changes and cavities difficult to measure. These limitations have given rise to optical based techniques like laser triangulation, confocal microscopy and low coherence interferometry. These methods are contactless and enable rapid 3D measurement data.

A Wyko optical profilometer (Veeco) was used to observe the device layer after etching the membrane. The profilometer uses the phase change of light reflecting from various heights of a similar material. The etch depth was compared with the number of steps to arrive at a etch rate per

step. The data was then used to target desired membrane thicknesses from the simulations. The resulting membranes were then compared with the target thicknesses to study the reliability of the process. Image profiles were also used to qualitatively assess both the sidewall angle and the membrane surface quality.

Characterizing the Sensor

Mechanical testing is essential to quantifying the performance of a sensor. The limiting factor is developing a method that can acquire useful data. FemtoTools is a Swiss company that specializes in the design and fabrication of highly sensitive MEMS tools for micro-force sensing. The goal of the mechanical tests was to use a sensing probe to measure the applied force vs. displacement relationship as well as the total travel distance of the membrane.

Testing Setup

The FT-MTA02 Micromechanical Testing and Assembly Station from FemtoTools AG was used with an FT-S Microforce Sensing Probe.

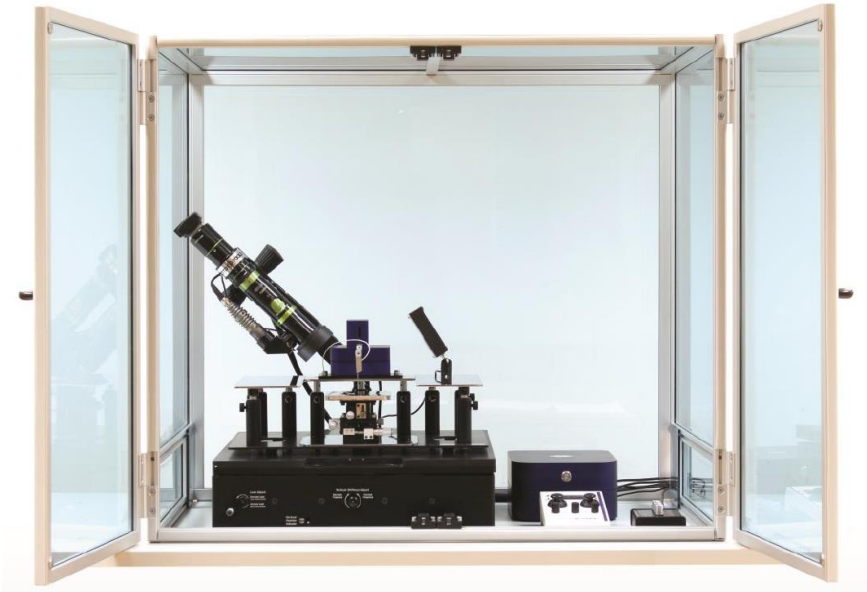

Figure 46 - FT-MTA02 Micromechanical Testing and Assembly Station

The sensing probe is a comb drive capacitive actuating bulk silicon device that can act as both an actuating and force sensing probe. The applied bias voltage and capacitance readout are used to

determine the applied force and micro position of the probe, while bulk movements are recorded by the servomotor located in the arm holding unit.

Figure 47 - FT-S Microforce Sensing Probe

The probe tip is made of tungsten and has a diameter of 50um. The probe needle was positioned in the center of the membrane.

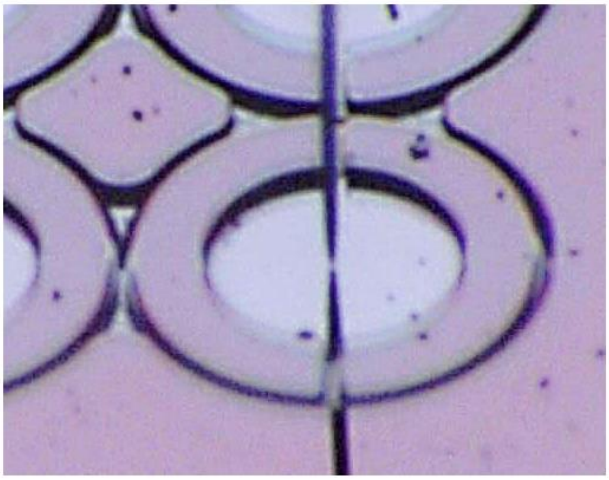

Figure 48- Tungsten Probe in contact with 360um membrane

The probe was used to displace the membrane until it came into contact with the fixed electrode, while measuring the resulting force.

Results

A 3um thick circular diaphragm with a diameter of 180um was used for the experiment. From the FEM simulations, the diaphragm was expected to display nonlinearities as the deflection increased due to the built up stress within the membrane material. The results are displayed below.

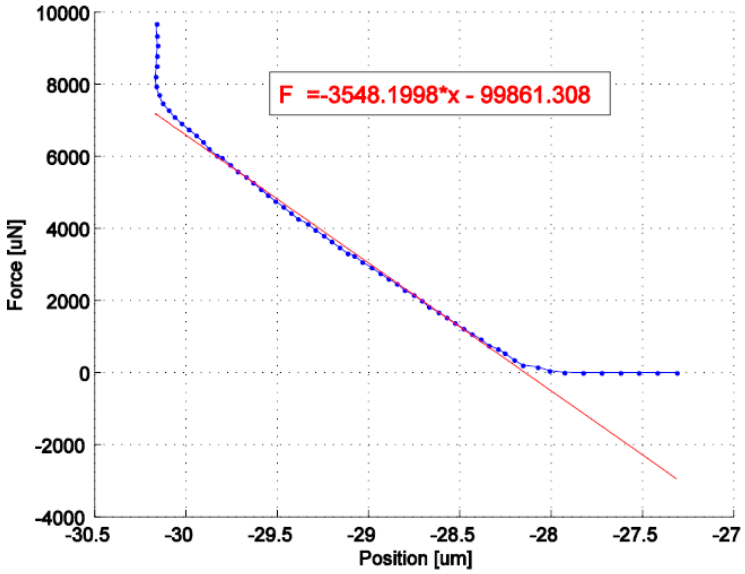

Figure 49 – Trial 1: Mechanical Deflection Curve of 360um diameter 3um thick membrane

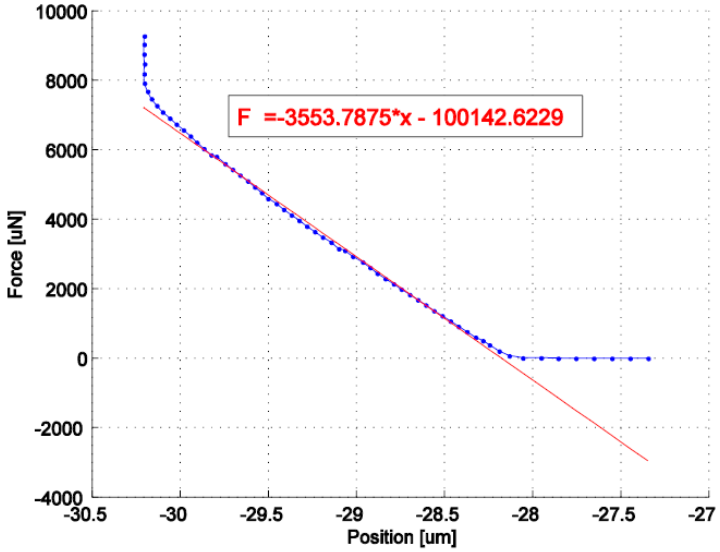

Figure 50 – Trial 2: Mechanical Deflection Curve of 360um diameter 3um thick membrane

The deflection maintains very good linearity through the entire measurement range with a slope of 3553N/µm or inversely 281µm/N. These results were compared to a simulation using a central force on the pressure sensor with a diameter of 360um and thickness of 3um. The simulation predicted a slope of 286.6 um/N. These measurements are in good accordance with simulation results.

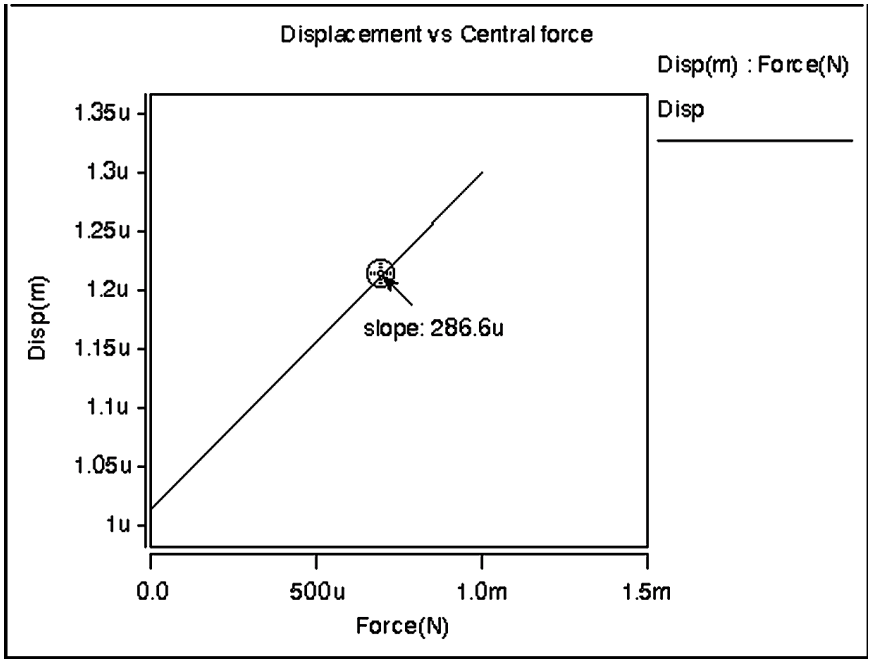

Figure 51 - Simulation of pressure sensor (360um dia., 3um thickness) using a central load

It should be noted that central loading of the membrane is not an accurate representation of the actual mechanical behavior. However, the central loading test can be used to illustrate the mechanical performance between the actual and simulation results.

The mechanical test could be improved by using a probe with a larger spherical tip. The spherical tip would be used to spread out the pressure over a greater portion of the membrane. This method could be used in future studies. Once the methodology is well established, the experiment is repeated over the entire sample size to properly characterize the mechanical response of the membrane.

Measuring the Pressure Sensor Response

Once the pressure sensors have been mechanically characterized the final step is to use them to measure pressure. The capacitance to pressure relationship was characterized using a pressure chamber, a pump and a reference gauge device. A capacitance to digital convertor was used to transfer the capacitance readout to a computer. Matlab code was developed to graph the capacitance signal in real time. Later, a wireless interface was created using Bluetooth enabled Rfduino's communication devices. The data was logged on a computer and the calibration curve for each sensor was created. This data was later compared with the FEM results to help improve the computer model.

Testing Setup

Pressure range, dimensions and functionality were all considered when designing the pressure chamber. The chamber was designed to handle the wide pressure sensing ranges of the three applications for which these sensors were designed, biomedical, environmental and industrial applications. The total range is 50kPa to 1200kPa. In order facilitate transport and enable live demos the goal of the chamber was to make it as compact as possible. This also minimized the amount of volume within the chamber which made varying the pressure easier. From a functionality perspective the chamber had to be easy to operate, protect the sensors (especially the wire bond connections) during transport and see through to help diagnose problems while improving visual appeal during live demonstrations.

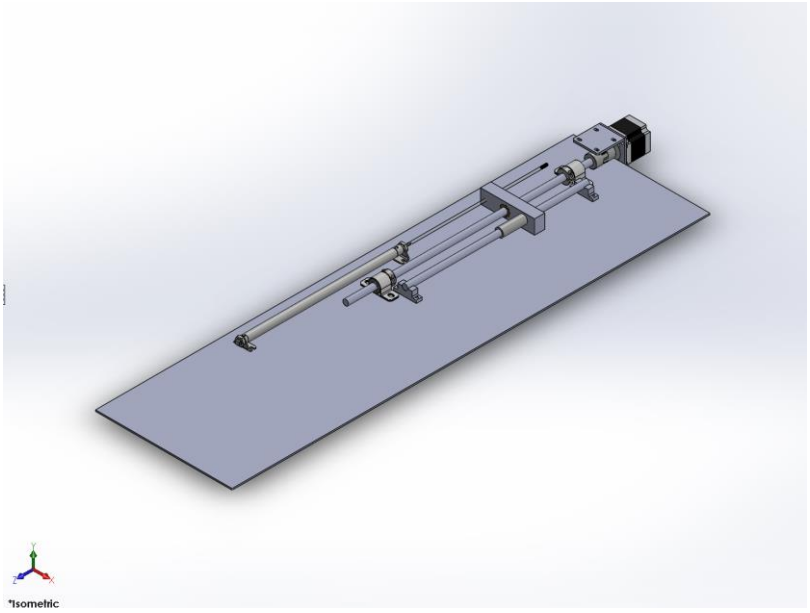

Figure 52 - Drawing of Automated Pressure Piston Setup

The system consisted of a double acting round body cylinder with one end attached to the chamber. A pressure gauge was mounted to the chamber to help calibrate the sensor. Since this was a closed system, as the cylinder decreased in volume, the pressure within the chamber increased and vice versa. In order to limit the size of the overall system, the chamber had to be made as small as possible. The area of the chamber as well as the measurement pressure range of 50kPa to 1200kPa was used to calculate the volume of the round body cylinder. Since air is a compressible fluid Equation (20) as given below was used,

$$P_1V_1 = P_2V_2 \ (20)$$

The total fixed volume was approximated at 1.4cm^3, therefore total volume needed was 17cm^3 to reach the maximum pressure of 1200kPa and therefore 34cm^3 to reach the minimum pressure of 50kPa. From these values, a cylinder with the smallest available bore size was chosen to minimize the amount of reaction force on the piston at 1200kPa. A cylinder with a bore size of 1.4cm was chosen with a stroke length of 25.4 cm. This allowed flexibility in organisation of the testing setup since the total volume within the cylinder was larger than what was required.

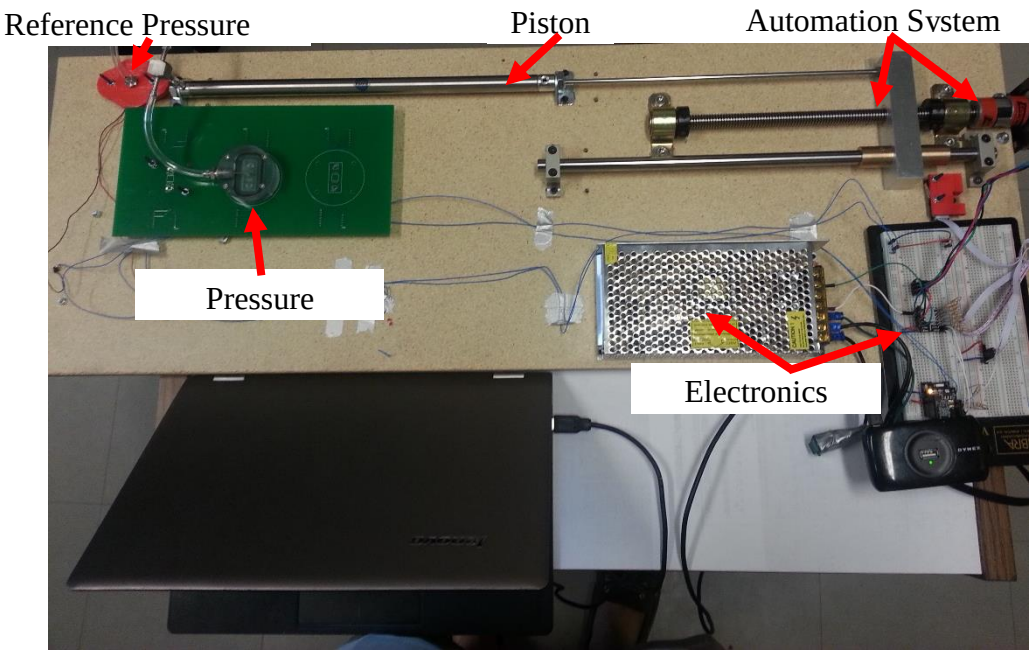

Figure 53 - Pressure Sensor Testing Setup

The chamber was machined out of clear Lexan. A second piece of Lexan below the PCB offered more mechanical support at high pressures. The chamber was attached to a PCB using four bolts and an O-ring provided the required air tight seal. The system was developed to deliver the required pressures over the entire measurement range. An electrical absolute piezoresistive pressure sensor was used to measure the pressure within the chamber. The absolute pressure sensor (MS5803-14BA) came in a water resistant package used primarily for monitoring water depth. This pressure sensor was chosen to make the set up compatible for water testing, which will be useful in the second phase of testing with coated sensors.

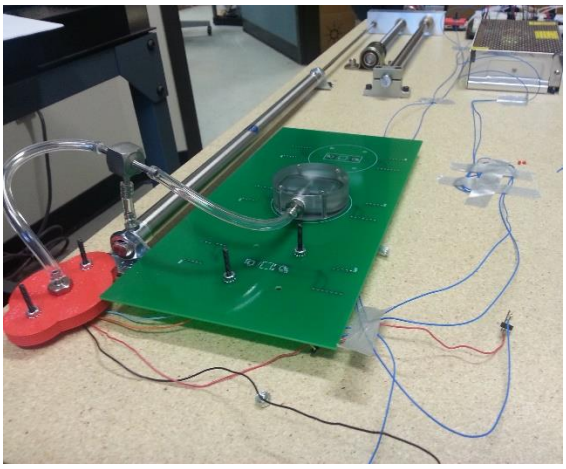

Figure 54 - Close up of Pressure Connection Set up and Pressure Chamber

Once the system was built we realized that tubing connections have a significant effect on the total fixed volume of the system. Our volume was found to be 3.1cm^3 therefore the total volume needed was 36.7cm^3 to reach the maximum pressure of 1200kPa and therefore 73.4cm^3 to reach the minimum pressure of 50kPa. Also by automating the testing set up, we had to limit the stroke length of the piston to 95% of its full value. These two shortcomings resulted in our system being able to produce a maximum pressure of 600kPa. A new iteration of the set up will incorporate a piston cylinder with >80cm^3 to ensure that it will be capable of reaching the pressures required for certain applications.

Logging the Sensor Data

The capacitive to digital convertor was used to acquire the capacitive signal from the pressure sensor. This data was sent to a wireless Rfduino device, which transmitted the data to a PC. A Matlab code on the PC was used to command, acquire and display the capacitive data from the pressure sensor in real time. This capacitive signal was then correlated with the mechanical compound gauge to get a correlation between capacitance and pressure. This system is also Bluetooth compatible, which will allow for wireless transmission of data in subsequent test phases.

Results

The current test set up has only recently been assembled and requires some debugging. Once the debugging phase is complete, data will begin to be collected from the pressure sensors. This data will be added to subsequent papers and will be used to fine tune the FEM model.

Table 10 - Comparative Chart between our expected Pressure Sensor Performance Values and Commercial Pressure sensors from page 21-32.

Product		Transduction	Application	Type	Range	Resolution (kPa)	Accuracy	Current Consumption	Output	Size	Cost
GE (Novasensor)	*NPC-100*	Piezoresistive	Medical	Gauge	-4kPa to 40kPa	N/A	+/- 1.0%	2mA	Analog	8.0 x 10.4 x 4.06 mm	$10- $5
	NPA-201	Piezoresistive	Consumer	Absolute	26kPa to 126kPa	1.5E-03	+/- 1.0%	35uA	Digital (I2C)	2.0 x 2.5 x 1mm	$5 - $2
	NPA-SPI	Piezoresistive	Industrial	Absolute	100 to 700kPa	2.4E+00	+/- 2.6%	400uA	Digital (SPI)	10.3 x 9.5 x 3.2mm	$17-$10
Murata (VTI Technologies)	*SP1000*	Capacitive	Barometer	Absolute	30kPa to 120kPa	1.0E-03	+/-0.2%	6.3uA	Digital (I2C)	6.1 Dia. x 1.7mm	--
Freescale	*MPL3115A2*	Piezoresistive	Altimeter	Absolute	50kPa to 110kPa	5.7E-05	+/- 0.7%	40uA	Digital (I2C)	5.0 x 3.0 x 1.1mm	$5.11-$2.50
Tronics Microsystems	--	Capacitive	Medical	Absolute	70kPa to 130kPa	1.0E-03	+/- 0.2%	160uA	Digital (I2C)	7.0 Dia. x 4.0mm	--
Bosch Sensortech	*BMP280*	Piezoresistive	Consumer	Absolute	30kPa to 110kPa	1.0E-03	+/- 1.0%	7uA	Digital (SPI,I2C)	2.0 x2.5 x0.9mm	$3.94-$1.5
McGill University	*R180*	Capacitive	Medical	Absolute	50kPa to 130kPa	1.2E-02	+/- 0.7%	3.3uA-24uA	Digital(SPI,I2C)	2.0x2.0x0.8mm	--
	R150	Capacitive	Environmental	Absolute	111kPa to 352kPa	1.0E-02	+/- 1.5%	3.3uA-24uA	Digital(SPI,I2C)	2.0x2.0x0.8mm	--
	R105	Capacitive	Energy Extraction	Absolute	111kPa to 1050kPa	1.1E-01	+/- 0.9%	3.3uA-24uA	Digital(SPI,I2C)	2.0x2.0x0.8mm	--

Optimization

Membrane Control

The short exposure low RF power etch (SELP) is the most critical etch step of the entire process. This step must be well controlled as any variation in thickness has an $1/s^3$ effect on the deflection. The SELP etch rate is dependent on the conditions within the chamber. The chamber can be controlled by running long high power cleaning steps before introducing the samples. These steps helps condition the surface of the target wafer and remove any residue that may have been left over from previous etches within the chamber. Proper cleaning helps improve the repeatability and controllability of the process. The data from etches are used to make adjustments for the number of etch steps needed to produce certain membrane properties. Table 9 compares the actual to expected membrane thickness based on the etch rates calculated in previous runs.

This iterative process was based on the assumption that the etch rate is repeatable between trial runs. An optical profiler was used to measure the etch depth of the device layer. The original etch rate was approximated at 0.5um/step. However, the trial results found the etch rate was lower than expected at 0.44um/step. This etch rate represents the minimum membrane thickness resolution that can be achieved with the current SELP process. The etch rate was used to determine the number of steps needed to achieve target membrane thicknesses of 2 and 5um.

	Etch Depth (um)			*Etch Rate (um/step)*	
Trial	**Target**	**Expected**	**Actual**	**Target**	**Actual**
1	25	25	20.3	0.5	0.45
2	25	25.3	24.8	0.45	0.44
3	28	27.9	27.9	0.44	0.44
4	25	24.8	24.8	0.44	0.44
5	28	27.9	27.5	0.44	0.44

Table 11 - SELP Etching Iterative Results

In Trial 5 of Table 9 there is small variability between the expected and measured results. This is due to changing chamber conditions. This variability can be mitigated by increased chamber cleaning or by using dedicated chambers for a specific task to hold environmental effects constant. Also, the use of automated production systems will increase repeatability by limiting human manipulation error.

Conclusions and Future Work

A new method for manufacturing absolute capacitive pressure sensors was developed using MIDIS^{TM}, a commercially available process offered by Teledyne DALSA. The method takes advantage of the clean vacuum and low leak rate of 45 molecules/s ($7.5E^{-13}$ atm·cc/s) [2, 3] as a highly stable reference. The method is also compatible to be manufactured alongside 3-axis accelerometers and 3-axis gyroscopes opening the possibility of 10-axis IMUs on a single dye [4]. A method for characterizing the mechanical properties of the sensing membrane using FT-MTA02 Micromechanical Testing and Assembly Station by FemtoTools showed an accurate correlation of membrane deflection constant with simulated results. Finally, a testing set up was designed and built to measure the electrical performance of the pressure sensors under the biomedical, environmental and energy extraction applications. This pressure testing set up will be used to compare sensor data from sensors with diameters ranging from 210-360um with membrane thicknesses of 3 and 5um. The data will be valuable in showcasing the range and versatility of this method for manufacturing absolute pressure sensors.

Design Improvements

Increasing Yield

One of the downsides of dry etching rather than wet etching the membranes is the bull's eye effect. The bull’s eye effect is caused by an increased concentration of reactive radical fluorine ions on the periphery of the wafer due to the less reactive aluminum chuck, which holds the wafer in place during the etching process. These effects can be mitigated using a consumable chuck, however this approach increases the cost and variability between runs by adding another variable to the etching process. Our approach to mitigate these effects is to decrease the diameter of the capacitive pressure sensors along the periphery of the wafer. This approach requires understanding the

relative difference between the constant etch rate, the etch rate along the periphery as well as the size of this transition zone. A further study on the specific machines that will be used will be important when scaling up production.

Etch Rate Optimized Designs

The SELP etch rate resolution has a direct effect on the membrane thickness. Since the thickness is dependent on a multiple of the etch rate resolution, the application specific pressure sensors should take this into account. Further optimization will be needed to improve the performance of the pressure sensors for biomedical, shallow water and deep water applications.

Diameter Optimized Designs

Another approach that could be useful is to keep a constant membrane thickness and change the diameter based on the application the pressure sensor will be used for. This approach is interesting because devices for different applications can be made in parallel on a single wafer. However, using this approach limits the flexibility of the current process reducing its advantages to a wet etch approach.

Playing with Geometry

Bossed Structures

As explained in the Capacitance Transduction section, bossed diaphragms can improve the linearity of the capacitive signal. The center of a bossed diaphragm remains parallel with the fixed electrode during the entire deflection range. Allowing the system to be simplified to Equation 14. The rate of deflection is determined by the width and thickness of the outer portion of the membrane.

Bossed structures can be made in the MIDIS^{TM} process by DRIE etching the top side of the device layer before the final bonding step. This is a step that is already available in the standard MIDIS process. The depth of etching will need to be precisely controlled and quantified in order to understand the SELP depth.

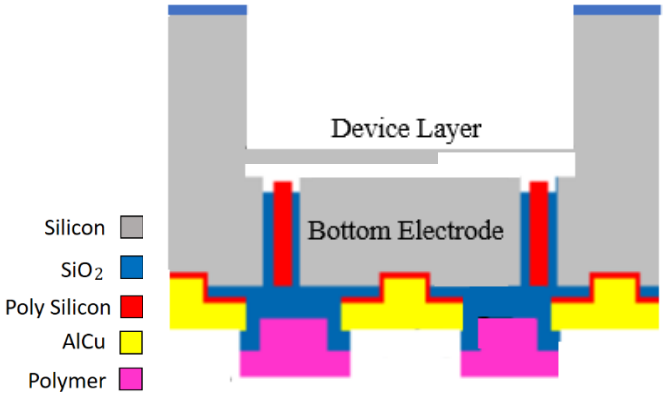

Figure 55- Bossed Pressure Sensor in MIDIS™

This method will increase linearity by simplifying the membrane dynamics. Special attention will need to be placed on the size of the bossed structure since it may be susceptible to acceleration artifacts.

Comb Diaphragms

As explained in the Capacitance section, embedded comb diaphragms can also increase linearity. The principle uses change in overlapping surface area (*A*) to determine the capacitance of the system in Equation 14. Each comb amplifies the signal. The dynamic range is also increased as the device is no longer limited by the distance between the electrodes.

Embedded Comb Diaphragms can be made in the standard MIDIS™ process. The top side of the device wafer as well as the bottom electrode is DRIE etched to create the comb pattern before the final bonding step. The number of combs are limited by the aspect ratio of the DRIE. Like in the bossed diaphragms, the depth of etching will need to be precisely controlled and quantified in order to understand the SELP depth.

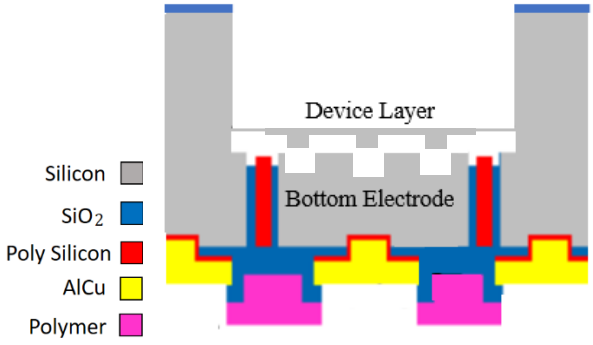

Figure 56 - Embedded Comb Diaphragm in MIDIS™

Environmental Testing

The goal of environmental testing will be to evaluate the fully packaged performance of the pressure sensor. The tests will study the pressure-capacitance curve over the entire measurement range. The curves will be used to characterize the effects of different loading environments and compatible coatings. Short and long term studies will be conducted to optimize the packaged solution for environmental, energy extraction and biomedical applications.

Temperature Testing

The effects of temperature on the sensing solution will be studied by placing the pressure chamber system in an oven. The temperature will be tested from 0-80^{o}C. A pressure curve will be taken at incremental temperature steps. The test will be repeated using different coatings and environmental conditions.

Environmental & Energy Extraction

The environmental & energy extraction testing will follow similar sequences, but at different pressure ranges. The pressure chamber used in the air calibration tests will be repurposed for this test. The packaged solution will be placed in the pressure chamber and filled with distilled water. Air pressure will be applied to the system to measure the response of the pressure sensor. The test will be conducted over the environmental range (1-25m deep) and the energy extraction range (1-100m deep). The pressure vs. capacitance curve will be used to characterize the various device coatings. The tests will be conducted over a long period of time (1-6 weeks) to measure the hermetical properties of the coating. These tests will be repeated using saline solution to simulate ocean conditions as well as any other medium (oil, water at various temperatures) that may interact with the sensing system.

Biomedical

The next phase of testing will be to place the pressure sensors into biological environment. The pressure chamber will include a material resembling soft tissue. A piston which will be used to

increase the pressure of the soft tissue. Finally a small infusion pump will be used to simulate the circulatory system.

This test set up will help evaluate the pressure transducer under realistic conditions. Various coated sensors will be tested in both short (1-2 hours) and long term (1-4 weeks). This test will be used to choose the coating material as well as optimize the coatings thickness for the biomedical application.

Table of References

[1] K. Petersen, P. Barth, J. Poydock, J. Brown, J. Mallon, Jr., and J. Bryzek, "Silicon fusion bonding for pressure sensors," in *Solid-State Sensor and Actuator Workshop, 1988. Technical Digest., IEEE*, 1988, pp. 144-147.

[2] L. Ouellet, "Wafer-level MEMS packaging," ed: Google Patents, 2003.

[3] (23 January). *MEMS Integrated Design for Inertial Sensors (MIDIS)*. Available: http://www.teledynedalsa.com/semi/mems/applications/midis/

[4] C. T. Eric Mounier, Guillaume Girardin, "MEMS Markets: Status of the MEMS Industry 2015," 2015.

[5] S. Beeby, G. Ensell, M. Kraft, and N. White, *MEMS Mechanical Sensors*:

, 2004.

[6] S. Finkbeiner, "MEMS for automotive and consumer electronics," in *Solid-State Device Research Conference (ESSDERC), 2013 Proceedings of the European*, 2013, pp. 9-14.

[7] W. Ding, "MEMS: Pressure Sensor," 2013.

[8] M. J. Madou, *Manufacturing Techniques for Microfabrication and Nanotechnology*: Taylor & Francis, 2011.

[9] K. E. Petersen, "Silicon as a mechanical material," *Proceedings of the IEEE*, vol. 70, pp. 420-457, 1982.

[10] S. Middelhoek, A. Bellekom, U. Dauderstadt, P. French, W. Kindt, F. Riedijk, *et al.*, "Silicon sensors," *Measurement Science and Technology*, vol. 6, p. 1641, 1995.

[11] A. Ballato, "Piezoelectricity: history and new thrusts," in *Ultrasonics Symposium, 1996. Proceedings., 1996 IEEE*, 1996, pp. 575-583 vol.1.

[12] M. A. Hopcroft, *Temperature-stabilized silicon resonators for frequency references* vol. 68, 2007.

[13] D. Ballantine Jr, R. M. White, S. J. Martin, A. J. Ricco, E. Zellers, G. Frye, *et al.*, *Acoustic Wave Sensors: Theory, Design, & Physico-Chemical Applications*: Academic press, 1996.

[14] K. Lange, B. E. Rapp, and M. Rapp, "Surface acoustic wave biosensors: a review," *Analytical and Bioanalytical Chemistry*, vol. 391, pp. 1509-1519, Jul 2008.

[15] J. W. S. Rayleigh, "On Waves Propagated Along," *Proc London Math Soc*, vol. 17, pp. 4-11, 1885.

[16] R. M. White and F. W. Voltmer, "DIRECT PIEZOELECTRIC COUPLING TO SURFACE ELASTIC WAVES," *Applied Physics Letters*, vol. 7, pp. 314-316, 1965.

[17] H. Wohltjen and R. Dessy, "Surface acoustic wave probe for chemical analysis. I. Introduction and instrument description," *Analytical Chemistry*, vol. 51, pp. 1458-1464, 1979.

[18] R. Puers, "Capacitive sensors: When and how to use them," *Sensors and Actuators A: Physical*, vol. 37–38, pp. 93-105, 6// 1993.

[19] W. H. Ko and Q. Wang, "Touch mode capacitive pressure sensors," *Sensors and Actuators A: Physical*, vol. 75, pp. 242-251, 6/8/ 1999.

[20] Y. Zhang, R. Howver, B. Gogoi, and N. Yazdi, "A high-sensitive ultra-thin MEMS capacitive pressure sensor," in *Solid-State Sensors, Actuators and Microsystems Conference (TRANSDUCERS), 2011 16th International*, 2011, pp. 112-115.

[21] S. Renard, C. Pisella, J. Collet, V. Gaff, and J. L. Lauront, "Capacitive Pressure and Inertial Sensors by EPI-SOI Surface Micromachining," in *Proceedings of IEEE Sensors*, 2002, pp. 1385-1388.

[22] J. Thurau and J. Ruohio, "Silicon Capacitive Absolute Pressure Sensor Elements for Battery-less and Low Power Tire Pressure Monitoring," in *Advanced Microsystems for Automotive Applications 2004*, J. Valldorf and W. Gessner, Eds., ed: Springer Berlin Heidelberg, 2004, pp. 109-118.

[23] J. Ruohio and R. Åström, "Method for the manufacturing of a capacitive pressure sensor, and a capacitive pressure sensor," ed: Google Patents, 2007.

[24] D. F. Mitch Berkson, "Understanding and specifying sensata technologies capacitive pressure transducers," in *Sensata Technologies*, S. Technologies, Ed., ed, 2007.

[25] Y. Zhang and K. D. Wise, "Performance of nonplanar silicon diaphragms under large deflections," *Microelectromechanical Systems, Journal of*, vol. 3, pp. 59-68, 1994.

[26] E. V. Thomsen, K. Reck, G. Skands, C. Bertelsen, and O. Hansen, "Silicon as an anisotropic mechanical material: Deflection of thin crystalline plates," *Sensors and Actuators A: Physical*, vol. 220, pp. 347-364, 12/1/ 2014.

[27] W. P. Eaton and J. H. Smith, "Micromachined pressure sensors: Review and recent developments," *Smart Materials and Structures*, vol. 6, pp. 530-539, Oct 1997.

[28] K. Kasten, N. Kordas, H. Kappert, and W. Mokwa, "Capacitive pressure sensor with monolithically integrated CMOS readout circuit for high temperature applications," *Sensors and Actuators, A: Physical*, vol. 97-98, pp. 83-87, 2002.

[29] G. Lammel, S. Armbruster, C. Schelling, H. Benzel, J. Brasas, M. Illing, *et al.*, "Next generation pressure sensors in surface micromachining technology," in *Solid-State Sensors, Actuators and Microsystems, 2005. Digest of Technical Papers. TRANSDUCERS '05. The 13th International Conference on*, 2005, pp. 35-36 Vol. 1.

[30] K. Knese, S. Armbruster, H. Weber, M. Fischer, H. Benzel, M. Metz, *et al.*, "Novel Technology for Capacitive Pressure Sensors with Monocrystalline Silicon Membranes," in *Micro Electro Mechanical Systems, 2009. MEMS 2009. IEEE 22nd International Conference on*, 2009, pp. 697-700.

[31] B. P. Gogoi, D. J. Monk, D. W. Odle, K. D. Neumann, D. L. Hughes, J. E. Schmiesing, *et al.*, "Method of forming an integrated CMOS capacitive pressure sensor," ed: Google Patents, 2002.

[32] B. P. Gogoi and D. Mladenovic, "Integration technology for MEMS automotive sensors," in *IECON 02 [Industrial Electronics Society, IEEE 2002 28th Annual Conference of the]*, 2002, pp. 2712-2717 vol.4.

[33] H. Artmann, F. Schafer, G. Lammel, S. Armbruster, H. Benzel, C. Schelling, *et al.*, "Monocrystalline Si membranes for pressure sensors fabricated by a novel surface micromachining process using porous silicon," in *Mems Components and Applications for Industry, Automobiles, Aerospace, and Communication Ii*. vol. 4981, S. W. Janson, Ed., ed Bellingham: Spie-Int Soc Optical Engineering, 2003, pp. 65-70.

[34] B. Diem, P. Rey, S. Renard, S. Viollet Bosson, H. Bono, F. Michel, *et al.*, "SOI 'SIMOX'; from bulk to surface micromachining, a new age for silicon sensors and actuators," *Sensors and Actuators: A. Physical*, vol. 46, pp. 8-16, 1995.

[35] B. Diem and M. T. Delaye, "Pressure transducer comprising a sealed transducer with a rigid diaphragm," ed: Google Patents, 1999.

[36] S. Armbruster, F. Schafer, G. Lammel, H. Artmann, C. Schelling, H. Benzel, *et al.*, "A novel micromachining process for the fabrication of monocrystalline Si-membranes using porous silicon," in *TRANSDUCERS, Solid-State Sensors, Actuators and Microsystems, 12th International Conference on, 2003*, 2003, pp. 246-249 vol.1.
[37] V. Lehmann, "Macroporous Silicon," in *Electrochemistry of Silicon*, ed: Wiley-VCH Verlag GmbH, 2002, pp. 183-205.
[38] L. Ouellet and M. Chowdhury, "Method of making MEMS wafers," ed: Google Patents, 2010.
[39] R. Beaudry, "Deep reactive ion etching," ed: Google Patents, 2009.
[40] R. Horning, M. Weber, and B. Johnson, "MEMS device with thinned comb fingers," ed: Google Patents, 2006.
[41] A. M. Mahajan, L. S. Patil, J. P. Bange, and D. K. Gautam, "Growth of SiO2 films by TEOS-PECVD system for microelectronics applications," *Surface and Coatings Technology*, vol. 183, pp. 295-300, 5/24/ 2004.
[42] G. T. A. Kovacs, N. I. Maluf, and K. E. Petersen, "Bulk micromachining of silicon," *Proceedings of the IEEE*, vol. 86, pp. 1536-1551, 1998.
[43] J. A. Pelesko and D. H. Bernstein, *Modeling Mems and Nems*: CRC press, 2002.